Electrostatics at Soft Interfaces

Introduction

Electromagnetic interactions determine the structure, assembly, and properties of soft matter. Electrostatic interactions are described within the context of classical electrostatics and statistical mechanics, whereas electrodynamic interactions, such as van der Waals forces, are described by quantum field theory. Although the latter seem more exotic, and perhaps worthy of our attention for that reason, here we will focus on electrostatic interactions with the aim of understanding their role at soft interfaces. Interestingly, a recent review of long range interactions stated that

"*Perhaps the greatest surprise is the inadequacy of theories of polar and electrostatic interactions compared with the present-day sophistication in formulating and computing charge-fluctuation forces.*" (French et al. 2010)

Before starting our description of electrostatics, let's remind ourselves of a few examples where electrostatic interactions play an important role at soft matter interfaces.

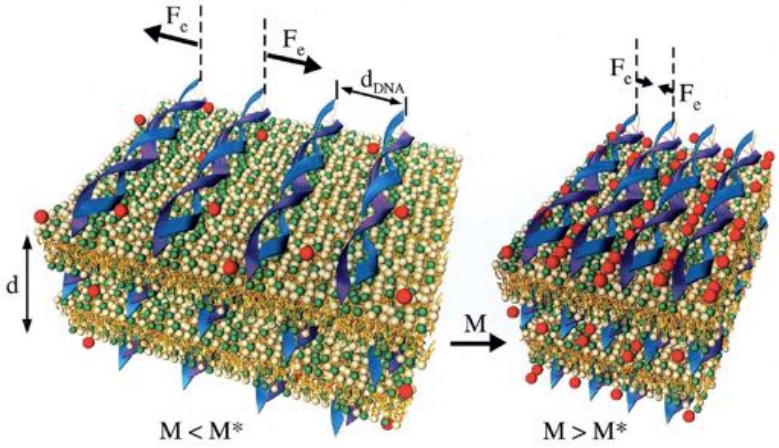

Figure 1 From (Koltover et al. 2000).

The left panel of Figure 1 shows an array of DNA molecules attracted to bilayer lipid membranes. Bare DNA is strongly charged with a negative charge every 1.7 Å along its length and the membranes contain positively charged cationic lipids. These attractive interactions are responsible for the ordered structure on the left in which the DNA are attracted to the membrane, but repelled from other DNA. The red dots are +2 charged mobile counterions. When present in sufficient concentration, $M > M^*$, the mobile divalent counterions mediate a transition to close packing of the DNA shown on the right side of Figure 1. The forces between the DNA molecules are now attractive.

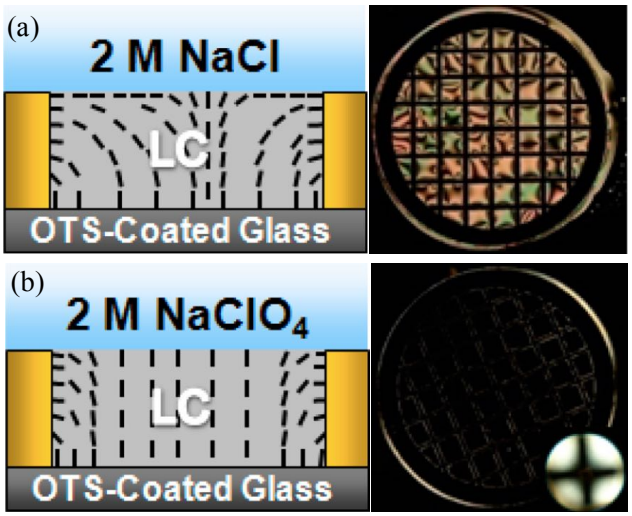

Figure 2 From (Carlton et al. 2012).

Figure 2 shows the interface between a liquid crystal material confined in square wells and the overlying aqueous electrolyte solution. The images on the right were observed through crossed optical polarizers that reveal the optical anisotropy of the liquid crystal. Substitution of one anion Cl^- for another ClO_4^- in the aqueous solution led to reordering of the liquid crystal. Such ion-specific effects are referred to as Hofmeister effects.

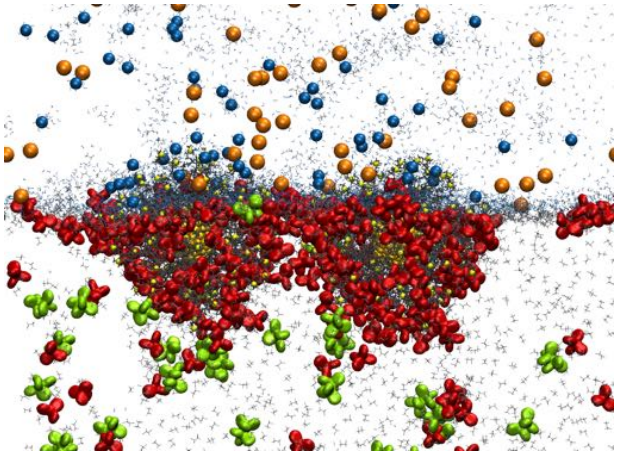

Figure 3 From (Bera et al. 2014).

Figure 3 shows two +100 charged nanoparticles at an interface between water on the top with blue (charge of -1) and orange (+1) ions and an organic solution on the bottom with red (-1) and green ions (+1). We can observe the very different ion distributions on the parts of the nanoparticle exposed to the top or bottom electrolyte solutions. Electrostatic interactions determine the position of nanoparticles within the interface and their voltage-tunable assembly.

There are numerous other interesting examples, but now we will start to discuss some basic theoretical ideas.

First, let's ask: when are electrostatic energies strong enough to have a substantial effect on structure and assembly of soft matter? Since $k_B T$ (Boltzmann's constant times the absolute temperature) is setting the scale for thermal energies that are relevant for soft materials, we can compare the electrostatic energy between two ions interacting across a continuum solvent (of relative permittivity or dielectric constant ε_r) to the thermal energy.

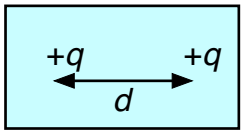

Setting the electrostatic energy equal to the thermal energy, we define the Bjerrum length,

Eq. 1 $$\ell_B = \frac{q^2}{4\pi\varepsilon_0\varepsilon_r k_B T}$$

When the distance between ions, *d*, is much larger than ℓ_B, then electrostatic interactions are weak compared to the thermal energy. Likewise, if ions are closer to one another than ℓ_B the electrostatic interactions dominate. For example, for two singly charged (monovalent) ions in water for which $\varepsilon_r \approx 80$, the Bjerrum length is 7 Å at room temperature ($T = 300$ K). Since a layer of water molecules usually surrounds ions in water, it is unlikely that two ion centers get much closer than 7 Å, therefore, electrostatic energies are at most comparable to $k_B T$. As the ion charge increases, so does ℓ_B. If q = +3, then $\ell_B \approx 63$ Å and electrostatic interactions can be much greater than $k_B T$ since the average distance between ions can be much less than ℓ_B, especially for ions near charged surfaces. Similarly, if ions are in an organic phase with $\varepsilon_r \approx 10$, then $\ell_B \approx 55$ Å for monovalent ions. Therefore, we expect similarly strong electrostatic effects for monovalent ions in an $\varepsilon_r \approx 10$ organic phase as for trivalent ions in water.

Now, we will start to investigate ensembles of ions in thermodynamic equilibrium. As we will see, this will generate a new length scale, the Debye length.

Poisson-Boltzmann Theory

(General references for this section are (Andelman 2006; Girault 2004).)

To address the electrostatics of electrolyte solutions, which contain ionic species (typically including both + and – charged ions) dissolved in a liquid solvent, we will first review the mean field Poisson-Boltzmann equation first introduced by Gouy and Chapman, then by Debye and Hückel. This equation can predict the distribution of + and – charged ions surrounding a charged species in solution, which could be one of the ions (Figure 4), or it could be a charged flat surface (Figure 4) or cylindrical wire that an electrochemist might want to use as an electrode, or it could be one of many oddly shaped bio-macromolecules or organized charged structures. Since the ion distribution underlies the

interactions between charged particles in electrolyte solutions, it is an appropriate place to start understanding the electrostatics of soft matter.

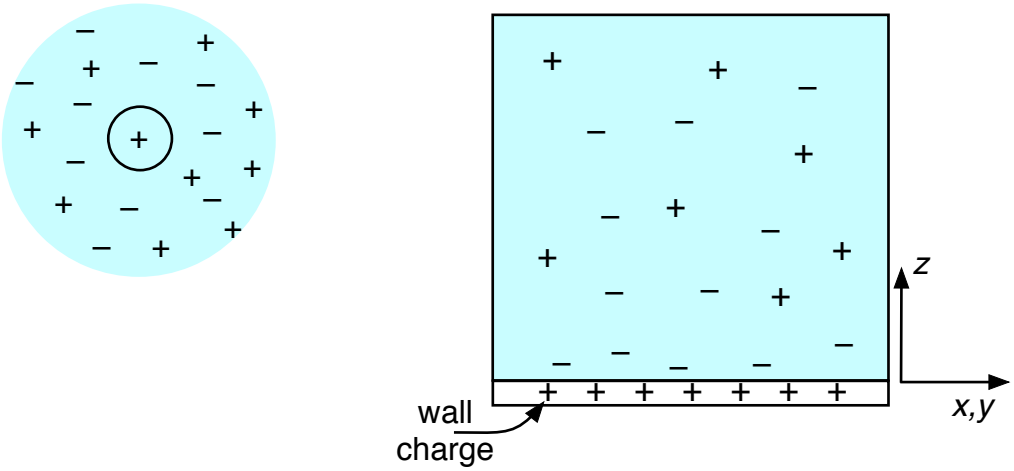

Figure 4

Poisson-Boltzmann theory is based upon a number of assumptions. The following is a slightly redundant list of assumptions.

1) Poisson-Boltzmann theory considers only Coulomb interactions between ions, and between an ion and a charged particle, wall, or surface. All other interactions are neglected.
2) The ions are taken to be point-like. Polarizability is neglected.
3) The solvent, for example water or liquid organics, is modeled as a continuous medium of relative permittivity (i.e., the dielectric constant) ε_r, whose uniform value is taken to be that of the pure solvent.
4) The electrostatic potential is a continuous function $\phi(\vec{r})$ due to the mean electrostatic field of all other ions.
5) The charge density (charge per volume) $\rho(\vec{r})$ and the ion concentration (or number density) $c(\vec{r})$ are continuous functions of $\vec{r}$

As a result of assumptions (1) and (2), all ions with the same charge behave the same way. The unique interactions of specific ionic elements that are due to the ion size, shape, and electronic structure are neglected.

Poisson-Boltzmann is a theory of mobile ions in thermodynamic equilibrium in a solvent. The spatial distribution of these ions can be adjusted by boundaries with a specified surface charge density (charge per area) or by boundary conditions on the electrostatic potential. A few options are shown below in Figure 5, where the boundary could take any shape.

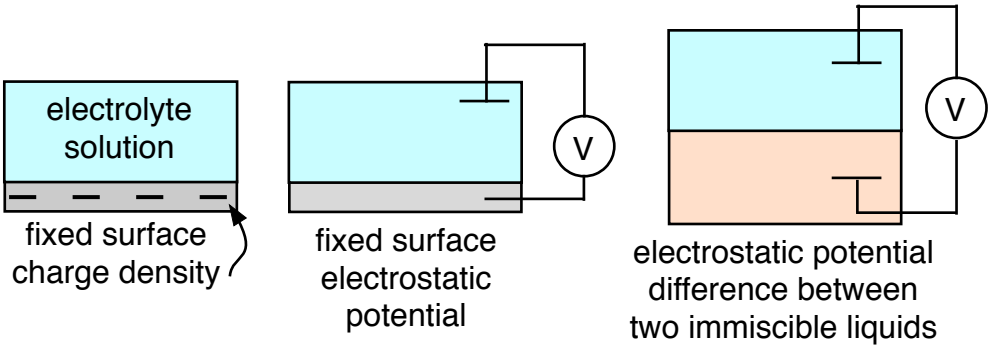

Figure 5

For this development of P-B theory, let's consider only two different types of ions, which will be labeled + and –, standing for positive and negative ions of charge Z_+ (> 0 for cations) and Z_- (< 0 for anions) whose concentration (or number density) is $c_+(\vec{r})$ and $c_-(\vec{r})$ with total charge density

Eq. 2 $$\rho(\vec{r}) = e\left[Z_+ c_+(\vec{r}) + Z_- c_-(\vec{r})\right] = \sum_i Z_i e c_i(\vec{r}),$$

where *e* is the elementary charge on an electron and the last expression refers generally to ions of type *i*.

Poisson's equation relates $\phi(\vec{r})$ to $\rho(\vec{r})$,

Eq. 3 $$\nabla^2\phi(\vec{r}) = -\frac{\rho(\vec{r})}{\varepsilon_0\varepsilon_r} = -\frac{1}{\varepsilon_0\varepsilon_r}\sum_i Z_i e c_i(\vec{r})$$

Here, I've neglected any position dependence of the permittivity. Ions in a liquid solution are mobile and adjust their position according to $\phi(\vec{r})$, which their position also influences. Having reached equilibrium, Poisson-Boltzmann theory assumes that they are arranged according to the following Boltzmann distribution for $c_\pm(\vec{r})$,

Eq. 4 $$c_\pm(\vec{r}) = c_\pm^{bulk}\exp\left[-Z_\pm e\phi(\vec{r})/k_B T\right],$$

where $c_\pm^{bulk}$ is a reference concentration for $\phi \to 0$. This assumption can be justified more formally in ways that reveal the approximations contained within it (and will be discussed later in these lectures). The Poisson-Boltzmann equation is the result of substituting Eq. 4 into Eq. 3,

Eq. 5 $$\nabla^2\phi(\vec{r}) = -\sum_{i=\pm}\frac{Z_i e c_i^{bulk}}{\varepsilon_0\varepsilon_r}\exp\left[-Z_i e\phi(\vec{r})\beta\right],$$

where $\beta = 1/k_B T$. Solutions of the Poisson-Boltzmann Eq. 5 provide an expression for $\phi(\vec{r})$ that determines the ion distributions $c_{\pm}(\vec{r})$ in Eq. 4. As a result of the approximations, there are limits to the applicability of Eq. 5, which will be discussed. It is most applicable to describing dilute electrolyte solutions of monovalent ions in highly polar solvents, such as water.

Debye-Hückel Theory of Ion Distributions about Ions in Bulk Solution

The Debye-Hückel theory was introduced to describe bulk electrolyte solutions. Here, we consider a central ion and solve the Poisson-Boltzmann equation in spherical coordinates, where the spherical symmetry of the situation leads to a solution for $\phi(\vec{r})$ as a function of the coordinate *r* only. This solution will demonstrate that an ionic cloud, or "ionic atmosphere", surrounds the central ion. The ionic cloud contains both + and – ions, but consists of primarily counterions, say – ions if the central ion is positive, which shield the charge of the central ion. An important insight from this theory is that although ions are, on average, distributed randomly throughout the electrolyte solution, each ion is screened by the local distribution of ions (Figure 6b).

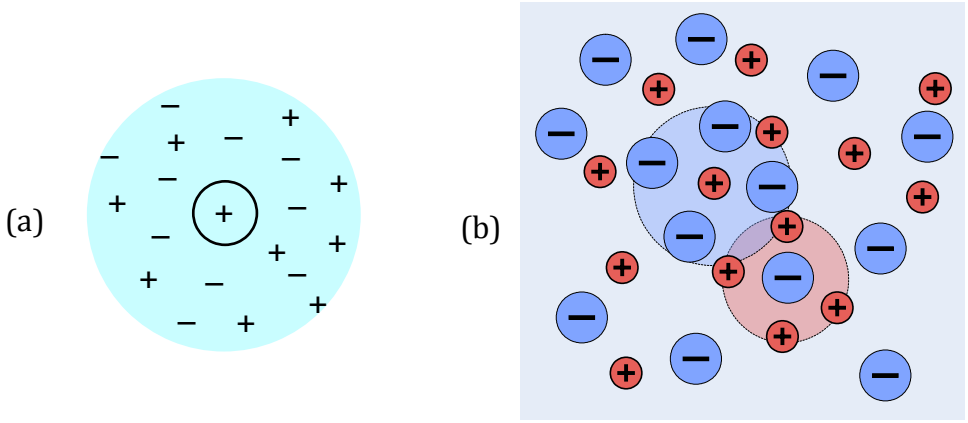

Figure 6 (b) from Wikipedia (by Roland Mattern)

Although an analytic solution of the full Poisson-Boltzmann equation in spherical coordinates is not available, Debye and Hückel provided a solution to the linearized P-B equation. When $Z_i e\phi \ll k_B T$ (or $\phi \ll 25$ mV for monovalent ions, $Z_i = \pm 1$),

Eq. 6 $$\nabla^2\phi(\vec{r}) \approx -\sum_{i=\pm} \frac{Z_i e c_i^{bulk}}{\varepsilon_0 \varepsilon_r}\left[1 - Z_i e\phi(\vec{r})\beta\right]$$

Electroneutrality of the solution requires that

Eq. 7 $$\sum_i Z_i c_i^{bulk} = 0\,.$$

Substituting the electroneutrality condition into Eq. 6 yields

Eq. 8 $$\nabla^2\phi(\vec{r}) \approx \frac{e^2}{\varepsilon_0 \varepsilon_r k_B T} \sum_{i=\pm} Z_i^2 \, c_i^{bulk} \, \phi(\vec{r}) \equiv \lambda_D^{-2} \, \phi(\vec{r}) \equiv \kappa^2 \, \phi(\vec{r}),$$

where the Debye length λ_D and the reciprocal Debye length κ are defined by Eq. 8. The Debye length will set the spatial extent of the ionic atmosphere about the central ion. Since any ion can be considered to be a central ion, λ_D can be used for any ion in solution. Equivalently, this spatial extent λ_D is the screening length to screen the charge of the central ion. It is convenient to remember a numerical expression for λ_D for the case of monovalent ions in water

Eq. 9 $$\lambda_D = \sqrt{\frac{\varepsilon_0 \varepsilon_r k_B T}{e^2 c^{bulk}}}$$ (for monovalent ions in water),

$$\lambda_D \approx \frac{3}{\sqrt{c^{bulk}\,[\mathrm{M}]}} \left[\text{Å}\right]$$

where we have taken the average concentration of ions in the bulk liquid to be $c^{bulk} = c_+^{bulk} = c_-^{bulk}$. If the electrolyte is a so-called strong electrolyte, which is completely dissociated when dissolved in the solvent, then c^{bulk} is the electrolyte concentration. The expression in Figure 22 leads to a Debye length $\lambda_D \approx 1$ nm for 0.1 M solutions, which is a physiologically relevant concentration for monovalent ions such as NaCl or KCl.

The mean field values of $\phi(\vec{r})$ and $\rho(\vec{r})$ are spherically symmetric, allowing Eq. 8 to be written in terms of the magnitude of *r*,

Eq. 10 $$\frac{d^2\left[r\phi(r)\right]}{dr^2} = \lambda_D^{-2}\left[\, r\phi(r)\right],$$

whose solution can be written as

Eq. 11 $$\phi(r) = \frac{C}{r} e^{-r/\lambda_D},$$

where we have used the boundary condition that $\phi(r) \xrightarrow[r\to\infty]{} 0$. The constant *C* is given by

Eq. 12 $$C = \frac{e Z_c}{4\pi\varepsilon_0\varepsilon_r}\left[\frac{e^{a/\lambda_D}}{1+(a/\lambda_D)}\right],$$

which can be derived using the condition for electroneutrality expressed as

Eq. 13 $$eZ_c + \int_a^\infty 4\pi r^2 \rho(r) dr = 0,$$

which states that the sum of the charge on the central ion, eZ_c, and all other ion charges must be zero. Here, the central ion is taken to have a finite size. The length *a* is the distance of closest approach of solution ions to the center of the central ion. Eq. 11 can be compared to the expression for the electrostatic potential about a single ion placed in a solvent which is not screened by additional ions,

Eq. 14 $$\phi_{\text{single}}(r) = \frac{eZ_c}{4\pi\varepsilon_0\varepsilon_r}\frac{1}{r},$$

which reveals that the primary effect of the other ions is to screen the electrostatic potential by $\exp[-r/\lambda_D]$.

The charge density has a similar dependence on *r* as the electrostatic potential,

Eq. 15 $$\rho(r) = -\frac{eZ_c}{4\pi\lambda_D^2}\left[\frac{e^{a/\lambda_D}}{1+(a/\lambda_D)}\right]\frac{1}{r}e^{-r/\lambda_D},$$

which also has the Debye length as the relevant length scale.

The Debye-Hückel theory has been used to derive a theoretical expression for the activity coefficients of ions, which has been shown to agree with experimental measurements for electrolyte concentrations up to 0.1 M. Additional information on the Debye-Hückel theory and its derivation can be found in the book by Girault (2004).

Gouy-Chapman Theory of Ion Distributions near a Charged Planar Surface

The Poisson-Boltzmann equation can be solved analytically in a system with planar symmetry, and is often referred to as Gouy-Chapman theory. Let's consider an ideal infinite planar surface with uniform surface charge σ at $z = 0$.

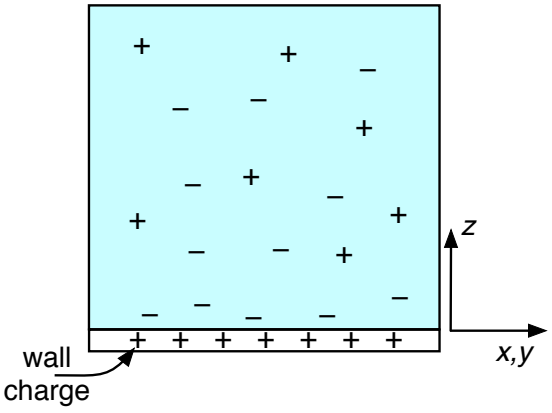

Figure 7

This system has translational invariance in *x* and *y*, which allows us to rewrite $c_{\pm}(\vec{r})$ as $c_{\pm}(z)$ and $\phi(\vec{r})$ as $\phi(z)$. The P-B equation is now an ordinary differential equation in *z*,

Eq. 16 $$\frac{d^2\phi(z)}{dz^2} = -\sum_{i=\pm} \frac{Z_i e c_i^{c^{bulk}}}{\varepsilon_o \varepsilon_r} \exp\left[-Z_i e\phi(z)/k_B T\right],$$

subject to the boundary condition at the charged surface,

Eq. 17 $$\left.\frac{d\phi(z)}{dz}\right|_{z=0} = -\frac{\sigma}{\varepsilon_o \varepsilon_r}$$

and the boundary conditions in the bulk solution given by

Eq. 18 $$\phi(z) \to \phi^{bulk} \text{ and } \frac{d\phi(z)}{dz} \to 0 \text{ as } z \to \infty.$$

The Gouy-Chapman equation, Eq. 16, can be solved analytically for ions of different charge, but here we will just present the solution for 1:1 monovalent ions, where 1:1 refers to (cation of charge 1*e* : anion of charge 1*e*). Rewriting $\frac{d^2\phi(z)}{dz^2}$ as $\frac{d}{d\phi}\left[\left(\frac{d\phi}{dz}\right)^2\right]$ and integrating once over $d\phi$ leads to an expression for the electric field (see Girault (2004) for a step-by-step derivation),

Eq. 19 $$\vec{E} = -\frac{d\phi}{dz}\hat{z} = \left(\frac{8c^{bulk}k_B T}{\varepsilon_o \varepsilon_r}\right)^{1/2} \sinh\left[\frac{e}{2k_B T}\left(\phi(z) - \phi^{bulk}\right)\right]\hat{z}$$

This expression can be used to relate the contact potential $\phi(z=0)$ to the surface charge density σ. Electroneutrality dictates that the surface charge is compensated by the solution charge,

Eq. 20 $$\sigma = -\int_0^\infty \rho(z)\, dz = \varepsilon_o \varepsilon_r \int_0^\infty \frac{d^2\phi(z)}{dz^2}\, dz = -\varepsilon_o \varepsilon_r \left(\frac{d\phi(z)}{dz}\right)_{z=0},$$

where Poisson's equation was used in the second integral, as well as the boundary condition, Eq. 18, in the final expression. Rewriting the derivative $d\phi(z)/dz$ using Eq. 19,

Eq. 21 $$\sigma = \left(8c^{bulk}k_B T \varepsilon_o \varepsilon_r\right)^{1/2} \sinh\left[\frac{e}{2k_B T}\left(\phi(0) - \phi^{bulk}\right)\right].$$

This relationship is illustrated in Figure 8, which shows that the contact potential $\phi(0)$ is on the order of a few tenths of a volt (when the reference potential in the bulk is chosen to be zero, $\phi^{bulk} = 0$) for three different solution concentrations. Note that a surface charge density of 0.3 C m^{-2} is equivalent to one charge per 0.5 nm^2. This is a typical value for a fully charged layer of singly charged lipids or surfactants at a planar surface. Note that typical potential differences are on the order of tenths of a volt. Calculating the electric field near the surface produces values of 10^7 to 10^8 V m^{-1}, which are given approximately by the potential difference divided by the Debye length, say 0.1 V / 1 nm.

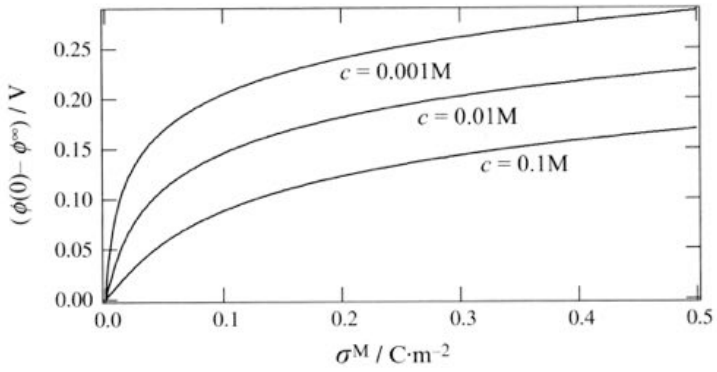

Figure 8 From (Girault 2004).

Further integration of $d\phi(z)/dz$ in the form given in Eq. 19 yields an expression for $\phi(z)$, given by

Eq. 22 $$\phi(z) - \phi^{bulk} = \frac{4k_B T}{e} \operatorname{arctan\,h}\left[e^{-z/\lambda_D} \tanh\left[\frac{e}{4k_B T}\left(\phi(0) - \phi^{bulk}\right)\right]\right]$$

The electrostatic potential $\phi(z)$ exhibits a simple monotonic decay (or increase, depending on the sign of the surface charge), as illustrated in Figure 9 for the case $\phi^{bulk} = 0$.

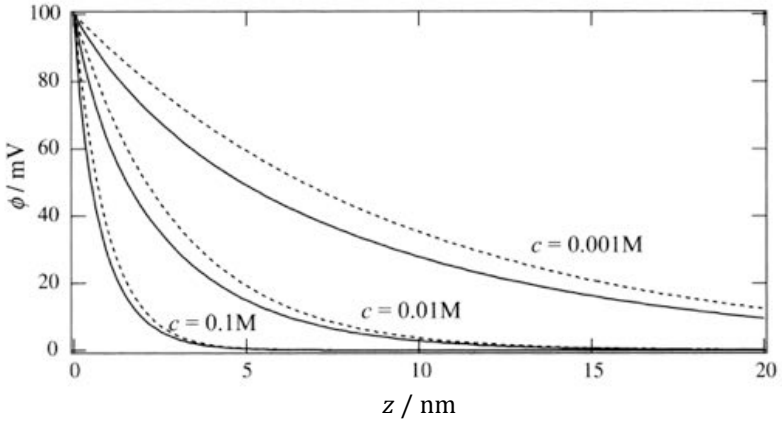

Figure 9 From Girault (2004).

Also illustrated by the dotted lines in Figure 9 are an exponential decay, $\phi(z) = \phi(0)e^{-z/\lambda_D}$, to demonstrate that the Debye length is also a good approximation for the decay of $\phi(z)$ near a planar charged wall. Recall that for 1:1 electrolytes $\lambda_D \approx 1$ nm for $c^{bulk} \approx 100$ mM, $\lambda_D \approx 3$ nm for $c^{bulk} \approx 10$ mM, and $\lambda_D \approx 10$ nm for $c^{bulk} \approx 1$ mM.

Substitution of $\phi(z)$ in Eq. 22 into the Boltzmann factor similar to that in Eq. 4 ($c_\pm(z) = c_\pm^{bulk} \exp\left[\mp e\phi(z)/k_BT\right]$), yields the ion distributions for the case $\phi^{bulk} = 0$,

Eq. 23 $$c_\pm(z) = c_\pm^{bulk}\left[\frac{1 \mp e^{-z/\lambda_D}\tanh[e\phi(0)\beta/4]}{1 \pm e^{-z/\lambda_D}\tanh[e\phi(0)\beta/4]}\right]^2.$$

These ion distributions vary monotonically as illustrated for a positively charged wall in Figure 10.

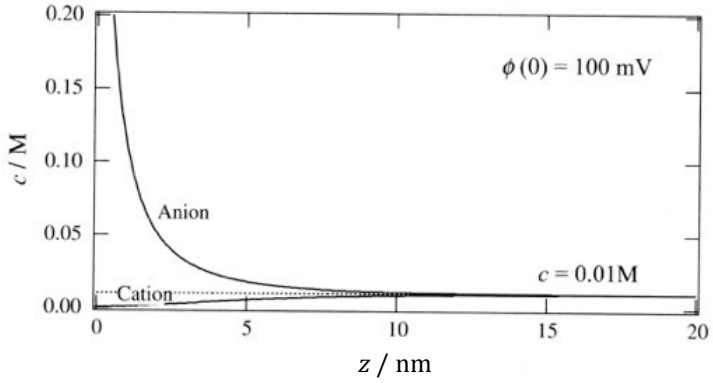

Figure 10 From Girault (2004).

Differentiation of the wall surface charge σ in Eq. 21 yields the differential capacitance per area, which electrochemists often refer to as the capacity, for the Gouy-Chapman theory,

Eq. 24 $$C_{GC} = \frac{\partial\sigma}{\partial[\phi(0) - \phi^{bulk}]} = \left(2c^{bulk}e^2\beta\varepsilon_o\varepsilon_r\right)^{1/2}\cosh\left[e\beta[\phi(0) - \phi^{bulk}]/2\right].$$

The capacity is usually measured by impedance spectroscopy by imposing a small amplitude AC variation on top of a larger DC electrostatic potential difference. Measuring the current response yields the complex impedance. Modeling the electrochemical system as an equivalent electronic circuit (with a capacitor as one of the elements) allows for measurements of the capacity. An example is shown in Figure 11 for the capacity of a liquid metal mercury electrode in a KF solution, along with the prediction of the Gouy-Chapman theory given by Eq. 24.

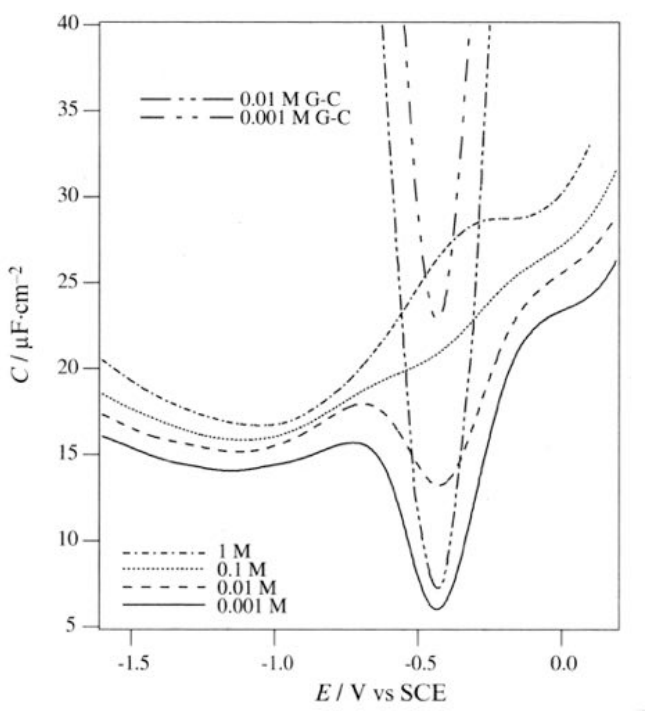

Figure 11 From Girault (2004).

The comparison in Figure 11 is not a fair test of the Gouy-Chapman theory because of the likely presence of a monolayer of water separating the liquid mercury and the electrical double layer (sometimes called the diffuse ion layer). The capacity of this adsorbed layer of water is referred to as the Helmholtz capacity C_H, reminiscent of the Helmholtz model of ion adsorption, which predated the Gouy-Chapman model, and assumed that a single layer of ions adsorbed to charged walls. In this case, the observed capacity C_{obs} will consist of two capacities in series, one due to the adsorbed layer, C_H, and the other due to the electrical double layer, C_{GC}, related as follows,

Eq. 25
$$\frac{1}{C_{obs}} = \frac{1}{C_H} + \frac{1}{C_{GC}}.$$

This expression shows that if C_H and C_{GC} are very different from one another, then C_{obs} will be nearly equal to the smaller of the two. We expect that C_{GC} is very small for values of $\phi(0) \approx \phi^{bulk}$, near the minimum of the C_{GC} curves shown in Figure 11. Alternatively, C_{GC} increases with bulk concentration c^{bulk}, so that a first approximation to C_H can be determined by the 1 M curve in Figure 11. Figure 12 shows the measured capacity at the lowest concentration from Figure 11 along with the prediction from Gouy-Chapman theory and the estimate of C_H using the capacitance data for the 1 M sample.

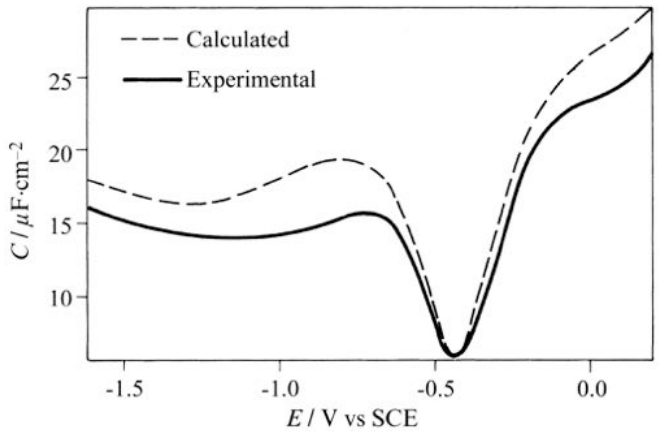

Figure 12 From Girault (2004).

Although the two curves in Figure 12 are much closer, the uncertainty in our knowledge of the adsorbed layer does not allow the Gouy-Chapman theory to be tested cleanly because we do not have a separate measurement of C_H. It is often found that measurements of capacity at the metal/solution interface are lower than the predictions of the Gouy-Chapman theory, C_{GC}.

An adsorbed layer of water is often referred to as a Stern layer. This has been incorporated within the Gouy-Chapman model by shifting the starting *z* position of the Gouy-Chapman ion distribution to be further from the surface of the charged wall. This *ad hoc* phenomenological model reduces the capacity from the Gouy-Chapman theory because the region of the ion distribution near the wall, which has the highest ion density, is removed. However, there is no clear guidance as to how much of this distribution should be removed.

More Experimental Phenomena

Ion-Specific Effects

Different types of ions, even of the same charge, generally behave differently. They have different solvation energies in water, they have different standard Gibbs energies of transfer, and they approach liquid surfaces and interfaces to different distances. An early and well-known effect was the observation by Hofmeister that different salts have different efficacy in precipitating proteins from solution. Hofmeister determined an ordered list of common anions and cations according to their ability to "salt out" proteins. A similar ordering has been observed in a great variety of situations. For example, the surface tension of aqueous electrolyte solutions exhibits an inverse Hofmeister effect. It was believed for a long time that Hofmeister effects were due to the ability of ions to encourage or discourage hydrogen bond formation, however, these ideas have recently been discredited. Current ideas include ion polarization, ion size and polarization of hydration shells, though further details are beyond the scope of this short course (Zhang and Cremer 2010; Levin et al. 2009). Ion-specific effects are not accounted for in Poisson-Boltzmann theory.

DNA Condensation and Ion Correlations

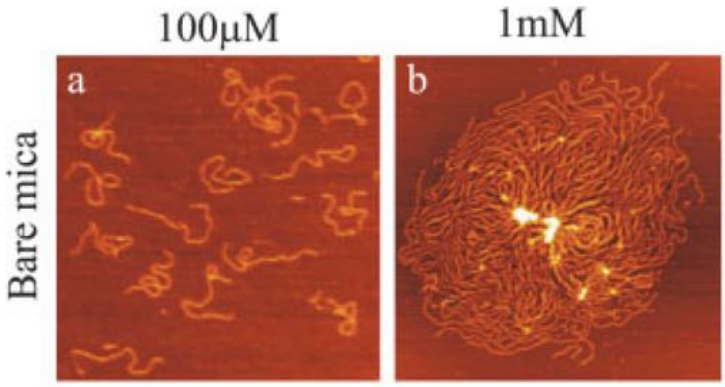

Figure 13 AFM images of DNA on mica at 2 different concentrations of spermidine ($[C_7N_3H_{22}]^{+3}$) in water. From (Besteman et al. 2007).

Figure 13 illustrates the condensation of DNA, a heavily charged polyelectrolyte, that occurs in the presence of a relatively small amount of a multivalent ion, +3, in the surrounding solution. Condensation has been observed for other charged polyelectrolytes, such as proteins. The particular image in Figure 13 was observed for DNA on a mica surface, but DNA condensation has been observed for DNA in bulk solution for a variety of multivalent ions. More highly charged ions usually required a lower concentration to trigger the condensation. Solutions of the Poisson-Boltzmann equation in spherical, planar, or cylindrical geometries demonstrate that charged particles, such DNA, will have their bare charge partially shielded, but the particle charge remains the same sign. So, that within the predictions of the Poisson-Boltzmann equation, the effective charge of DNA that includes its bare charges plus those surrounding it in the nearby solution, say within a Debye length, will remain negative and two DNA molecules will continue to repel each

other electrostatically. It has been shown that this repulsion should overcome any other attractive forces, such as van der Waals forces.

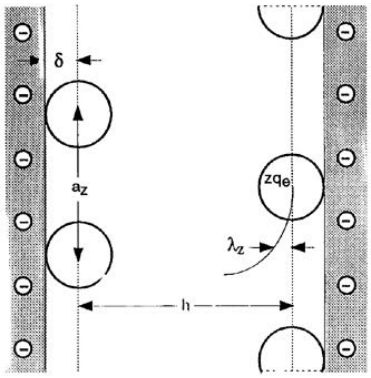

Figure 14 From (Rouzina and Bloomfield 1996).

Figure 14 illustrates the idea that ion correlations between two charged surfaces with mobile counterions can lead to an attractive interaction. A mobile ion (+*Ze*) on one surface can repel nearby mobile ions (+*Ze*) on the adjacent surface, leading to a correlation hole that exposes the underlying negative charge of the second surface, thus attracting the mobile ion from the first surface. Electrostatic ion correlations are greatly enhanced when the coupling strength, or strong coupling parameter, defined as the ratio of the Bjerrum length to the average distance between ions

Eq. 26 $$\Gamma = \frac{\ell_B}{d}$$

is greater than 1. As described in Eq. 1, the Bjerrum length scales as the product of the charges and is much larger for higher charged ions. Ion correlations are not included in the Poisson-Boltzmann equation.

Charge Reversal and Ion Correlations

It has been demonstrated that adding multivalent ions to solution can reverse the electrophoretic mobility of charged particles moving in an electric field. This has been interpreted as reversing the sign of the particle's charge.

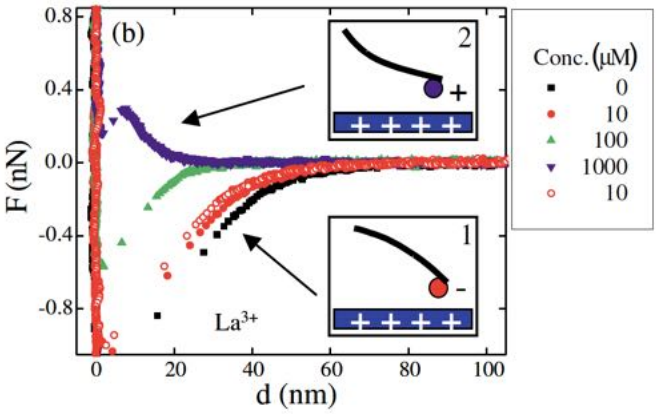

Figure 15 Addition of $LaCl_3$ to aqueous solution surrounding a silica sphere (negatively charged) on the end of an AFM tip interacting with a positively charged, amine-terminated, surface, from (Besteman et al. 2004).

More recently, AFM experiments have demonstrated that addition of multivalent ions can reverse the force on a small charged sphere within an aqueous solution, as shown in Figure 15. A zero temperature calculation of only the electrostatic energy of point-like ions surrounding a spherical charged particle illustrated that the lowest energy is obtained when there is an excess number of counterions that exceeds the bare (i.e., without counterions) charge of the particle (Figure 16). This excess leads to a reversal of the net charge of the sphere+counterions system. If the counterion charge were uniformly smeared out over the surface of the sphere, the lowest electrostatic energy would be achieved for a total charge of zero. Here, correlations in the positions of discrete counterion arranged on the sphere enable charge reversal.

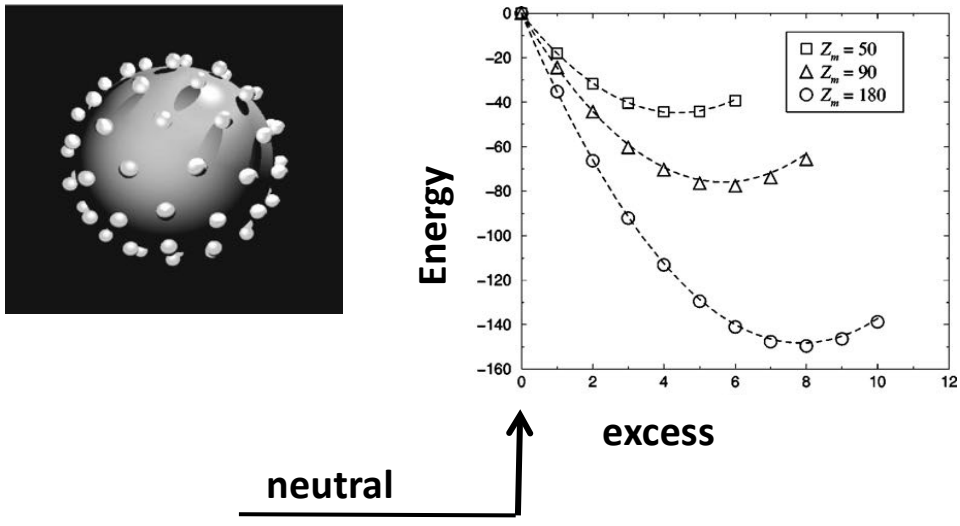

Figure 16 From (Messina et al. 2001).

Many Body Effects

Many experiments yield results that differ quantitatively from the predictions of the Poisson-Boltzmann equation, while others produce results that are qualitatively inconsistent. A number of different theoretical descriptions have been offered to resolve these discrepancies. Although a single generally accepted theory does not currently exist, I will present a pedagogical description (Kjellander and Greberg 1998) that introduces the role of many body effects and distinguishes these effects from the mean-field Poisson-Boltzmann theory. This approach relies on some ideas from the statistical mechanics of liquids, which I will review, and on a model system known as the primitive model of electrolyte solutions.

Primitive Model of Electrolyte Solutions

1. Ions as charged, hard spheres of diameter *a*.
2. The solvent (aqueous or organic) is a dielectric continuum of relative permittivity (i.e., the dielectric constant) ε_r.

In addition to the assumptions of the primitive model, we place the electrolyte solution against a smooth, hard, planar wall of infinite extent in $x-y$ with uniform surface charge σ. We will further assume that $\varepsilon_{r,wall} = \varepsilon_r$, which allows us to neglect image charge effects that would otherwise result from a dielectric discontinuity at the surface of the wall.

Except for the assumption that ions are hard spheres of finite radius, this system appears identical to that used by Gouy and Chapman when they introduced the Poisson-Boltzmann equation. However, the model that we will describe will not assume that ions interact only with the mean electrostatic field due to all other ions, as in the Poisson-Boltzmann equation. Although this model still neglects several features of importance for real systems, such as the molecular nature of the solvent and charged boundary (or soft interface), as well as different sizes and shapes of ions, we will see that the roles of many body effects on ion distributions near charged surfaces can be identified.

We will use the coordinate system shown in Figure 17.

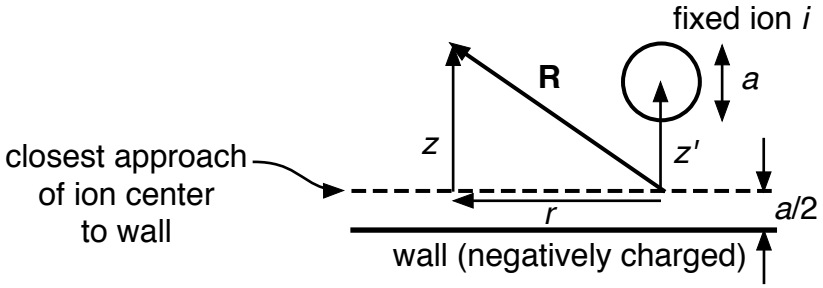

Figure 17

Potential of Mean Force

We introduce the potential of mean force that will be generally useful in the theory of liquids. Consider the potential of mean force $w_i(z')$ that acts on an ion of species *i* located at a distance z' from the charged wall, where the position of the ion is shown in Figure 17. The concentration of ions *i* at z' is given by a Boltzmann distribution

Eq. 27 $c_i(z') = C_i \exp[-\beta\, w_i(z')]$, where $\beta = 1/k_B T$.

The potential of mean force w_i^{bulk} is constant in the bulk solution, such that

Eq. 28 $c_i^{bulk} = C_i \exp[-\beta\, w_i^{bulk}]$,

which allows us to rewrite

Eq. 29 $c_i(z') = c_i^{bulk} \exp[-\beta\,(w_i(z') - w_i^{bulk})]$.

This might appear as if we have just used the same sort of Boltzmann distribution assumption that was used in Poisson-Boltzmann theory, but further consideration of the meaning of the potential of mean force shows that this formalism is exact. Take the logarithm of Eq. 29,

Eq. 30 $\ln c_i(z') = \ln c_i^{bulk} - \beta w_i(z') + \beta w_i^{bulk}$.

Adding a constant μ_i° to both sides, dividing by β, and rearranging, yields

Eq. 31 $\mu_i^{\circ} + k_B T \ln c_i(z') + w_i(z') = \mu_i^{\circ} + k_B T \ln c_i^{bulk} + w_i^{bulk}$.

Taking μ_i° to be the standard chemical potential of particle (ion) *i*, we see that $\mu_i^{\circ} + k_B T \ln c_i^{bulk}$ is the chemical potential of an ideal bulk solution of particles *i*, where the term "ideal" is used in the same sense as for an ideal gas, that is, there are no interactions between particles. The potential of mean force w_i^{bulk} accounts for the non-ideal behavior of the solution and is referred to as an excess chemical potential, $w_i^{bulk} = \mu_i^{ex,bulk}$.

Since the terms μ_i°, $k_B T \ln c_i^{bulk}$, and w_i^{bulk} on the right side of Eq. 31 are all constants, we have

Eq. 32 $\mu_i^{\circ} + k_B T \ln c_i(z') + w_i(z') = \mu_i = \text{constant}$,

which expresses the constancy of the chemical potential μ_i throughout the solution, for all z', at equilibrium.

The first two terms in Eq. 31, $\mu_i^{\circ} + k_B T \ln c_i(z')$, represent the ideal chemical potential of ion *i* at z'. The third term $w_i(z')$ is the z'-dependent excess chemical $\mu_i^{ex}(z') = w_i(z')$. Since the chemical potential is equal to the change in free energy upon addition of one particle (ion) to the system, we can write

Eq. 33

$$\Delta(\text{free energy}) = \text{Change in configurational (mixing) entropy (the ideal part)} + \text{Change in intermolecular interactions (the excess part, } w_i(z')\text{)}$$

The ideal part, $\mu_i^0 + k_B T \ln c_i(z')$, is the change in configurational (mixing) entropy that occurs upon releasing the particle *i* from coordinate z'. The excess part, $w_i(z')$, is the work done against interactions between the added particle (ion *i*) and the rest of the particles (ions) in the system, including those in solution and in the wall, when placing ion *i* at z' and holding it there.

From Eq. 29, $c_i(z') = c_i^{bulk} \exp[-\beta\,(w_i(z') - w_i^{bulk})]$, we can see that if $w_i(z') > w_i^{bulk}$, the concentration $c_i(z')$ is smaller than the bulk concentration because work must be done to place it at coordinate z', whereas when $w_i(z') < w_i^{bulk}$, the concentration $c_i(z')$ is larger than the bulk concentration and ions *i* want to go to the distance z' from the wall.

More generally, consider moving ion *i* from z'' to z':

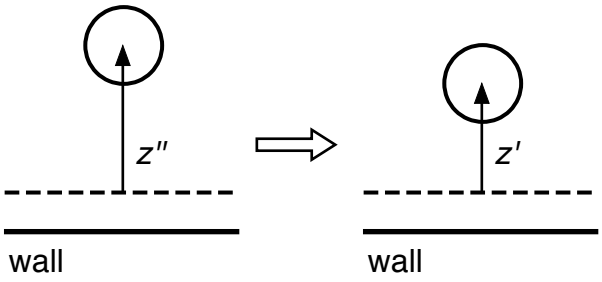

Figure 18

Since $-w_i(z'')$ is the work to remove ion *i* from z'', and $w_i(z')$ is the work to place ion *i* at z', the work to move ion *i* from z'' to z' is given by $w_i(z') - w_i(z'')$. We can see that the term $w_i(z') - w_i^{bulk}$ in Eq. 29, $c_i(z') = c_i^{bulk} \exp[-\beta\,(w_i(z') - w_i^{bulk})]$, is just the work to move ion *i* from the bulk to coordinate z'.

Thus, we can treat $w_i(z')$ as we would a z'-dependent potential energy. Thus, $-\dfrac{dw_i(z')}{dz'}$ is a force on ion *i* at z'.

Mean Force

Let F_0 be the free energy of the system without a fixed ion *i*, then $F_0 + w_i(z')$ is the total free energy of the system with ion *i* fixed at z', and the mean force $f_i(z')$ on ion *i* at z' due to all other ions is given by

Eq. 34 $$f_i(z') = -\frac{d[F_0 + w_i(z')]}{dz'} = -\frac{dw_i(z')}{dz'}.$$

In other words, $f_i(z')$ is the total force on ion *i* fixed at z' due to all other ions averaged over all possible configurations of the other ions. Note that the possible configurations depend upon the interactions of the mobile ions with the fixed ion *i* at z' and with the wall. So, for example, mobile ions that are attracted to the fixed ion *i* will have configurations that favor them being in the vicinity of ion *i*.

At this point, we will calculate the mean force on a fixed ion, $f_i(z')$. The usefulness of this will be to reveal the role of many body effects that influence the distribution of ions near a charged wall. Since the ion distribution underlies the electrostatic interactions between charged particles and a charged surface, such as that between a charged globular protein and a charged biomembrane, these calculations can also provide insight into the force experienced by a charged particle (the protein) in an electrolyte solution within the vicinity of a charged wall (the biomembrane).

To proceed further, consider the concentration of mobile ions *j* at $\vec{R} = (x, y, z)$ in the neighborhood of fixed ion *i*, which we call $c_j(\vec{R} \mid z', i)$. According to the geometry in Figure 17, which we reproduce here (with a slight addition of the distance *D*),

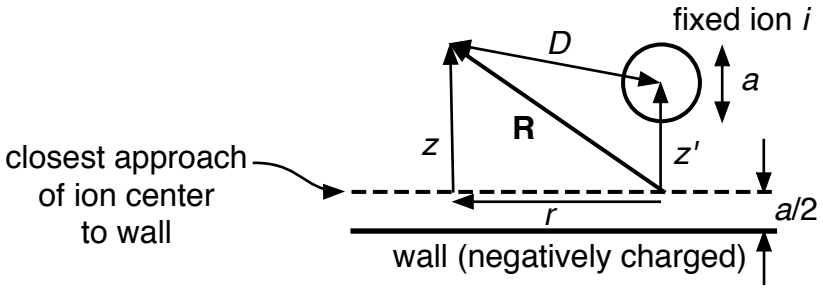

Figure 19

The distance $r = \sqrt{x^2 + y^2}$ with $\vec{r} = (x, y)$, and $\vec{R} = (r, z, \varphi)$ in cylindrical coordinates about the axis coincident with z'. Since the infinite wall is cylindrically symmetric, we let $\vec{R} = (r, z)$, so that we will write

Eq. 35 $$c_j(\vec{R} \mid z', i) = c_j(r, z \mid z', i)$$

to refer to the concentration of mobile *j* ions at the position (r, z) from a fixed ion *i* at coordinate z'.

The mean force on fixed ion *i* includes contributions from the wall, $v_i(z')$, and the mobile ions, $w_i^{mobile}(z')$, where the superscript *mobile* refers to all of the mobile ions,

Eq. 36 $$w_i(z') = v_i(z') + w_i^{mobile}(z').$$

The mean force on fixed ion *i* is written as

Eq. 37 $$f_i(z') = -\frac{dv_i(z')}{dz'} - \frac{dw_i^{mobile}(z')}{dz'},$$

where the first derivative is the force from the wall on fixed ion *i* and the second derivative is the mean force on fixed ion *i* from all mobile ions.

If we know the concentrations of all mobile ions, $c_j(r,z\,|\,z',i)$, and the interaction potentials between the fixed ion and the mobile ions, as well as the interaction potential between the fixed ion and the wall, then we can calculate $f_i(z')$.

Let $u_{ij}(D)$ be the pair interaction potential between the fixed ion *i* and a mobile ion *j* separated by a distance *D* (shown in Figure 19). Noting that only the *z*-component of the force is relevant because of the cylindrical symmetry, we write the *z*-component of the force on fixed ion *i* due to ion *j* at (r,z) as

Eq. 38 $$-\frac{\partial u_{ij}(D)}{\partial z'} = -\frac{\partial u_{ij}([r^2 + (z-z')^2]^{1/2})}{\partial z'},$$

where $D = [r^2 + (z-z')^2]^{1/2}$ as shown in Figure 19. The mean force $f_i(z')$ in Eq. 37 can be rewritten by expressing $w_i^{mobile}(z')$ as a sum over pair interaction potentials,

Eq. 39 $$f_i(z') = -\frac{dv_i(z')}{dz'} - \sum_j \int \frac{du_{ij}(D)}{dz'} c_j(\vec{R}\,|\,z',i)\,d\vec{R},$$

where the number of mobile ions *j* in the volume element $d\vec{R}$ is given by $c_j(\vec{R}\,|\,z',i)\,d\vec{R}$.

Note that if $c_i(z')$ is known, then $f_i(z')$ can be calculated from it, and vice versa. For example, Eq. 32 allows us to write

Eq. 40 $$f_i(z') = -\frac{dw_i(z')}{dz'} = -\frac{d[\mu_i - \mu_i^{\circ} - k_B T \ln c_i(z')]}{dz'} = k_B T \frac{d \ln c_i(z')}{dz'}$$

Alternatively, integrating this equation allows us to express $c_i(z')$ in terms of $f_i(z')$,

Eq. 41 $$\int_{z'}^{\infty} d\ln c_i(z'') = \ln c_i(\infty) - \ln c_i(z') = -\ln\left[\frac{c_i(z')}{c_i^{bulk}}\right] = \beta\int_{z'}^{\infty} f_i(z'')\,dz'',$$

which relates the ion concentration profile to the particle and wall interactions,

Eq. 42 $$c_i(z') = c_i^{bulk}\exp\left[-\beta\int_{z'}^{\infty} f_i(z'')\,dz''\right].$$

Similarly, starting from $f_i(z') = -dw_i(z')/dz'$, we can write the potential of mean force in terms of the integral of the mean force,

Eq. 43 $$w_i(z') = w_i^{bulk} + \int_{z'}^{\infty} f_i(z'')\,dz''.$$

As an aside, for those of you familiar with the pair distribution function, $g(r)$, say for a single species isotropic liquid phase, defined by $c(r) = g(r)c^{bulk}$, or by $c_j(r\,|\,i) = g_{ij}(r)c_j^{bulk}$ for two species in an isotropic bulk liquid phase, we can similarly define a pair distribution $g_{ij}(r,z,z')$ for the system under discussion by

Eq. 44 $$c_j(r,z\,|\,z',i) = g_{ij}(r,z,z')c_j(z).$$

Electrostatic and Hard-core Interactions

Here, we choose simple wall and pair interactions which allow us to calculate the mean force $f_i(z')$ in the primitive model from

Eq. 39 $$f_i(z') = -\frac{dv_i(z')}{dz'} - \sum_j \int \frac{du_{ij}(D)}{dz'} c_j(\vec{R}\,|\,z',i)\,d\vec{R}$$

Pair interactions between ions will be the sum of Coulomb electrostatic and hard sphere interactions

Eq. 45 $$u_{ij}(D) = u_{ij}^{el}(D) + u_{ij}^{core}(D),$$

where

Eq. 46 $$u_{ij}^{el}(D) = \frac{q_i q_j}{4\pi\varepsilon_o\varepsilon_r D} \quad \text{and} \quad u_{ij}^{core}(D) = \begin{cases} \infty & D < a \\ 0 & D \geq a \end{cases}$$

where all the ion species have the same diameter *a*.

The ion-wall potential is

Eq. 47 $$v_i(z) = \frac{-q_i(z+b)\sigma}{2\varepsilon_0\varepsilon_r},$$

where charge on the wall is located at $z = -b$ as shown in Figure 20.

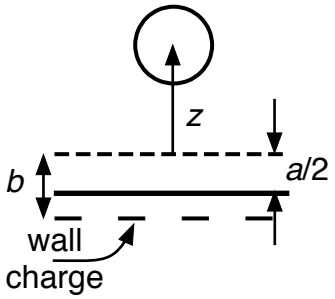

Figure 20

Next, we write the force as a sum of the electrostatic piece and the hard core repulsions,

Eq. 48 $$f_i(z') = f_i^{el}(z') + f_i^{core}(z').$$

We write the electrostatic part in terms of the total charge density in the neighborhood of ion *i*,

Eq. 49 $$\rho(r,z\,|\,z',i) = \sum_j q_j\, c_j(r,z\,|\,z',i),$$

and, skipping some calculations,

Eq. 50 $$f_i^{el}(z') = q_i\left[\frac{\sigma}{2\varepsilon_0\varepsilon_r} - \int \frac{z-z'}{4\pi\varepsilon_0\varepsilon_r D^3}\,\rho(r,z\,|\,z',i)\,d\vec{r}\,dz\right].$$

The electrostatic part of the mean force on fixed ion *i*, $f_i^{el}(z')$, consists of two parts. The first is just the product of the charge q_i and the electrostatic force from the wall (where $\sigma / 2\varepsilon_0\varepsilon_r$ is the electric field of the wall of surface charge density σ). The second is simply q_i times the integral of the Coulomb force from all the mobile ions, where $1/4\pi\varepsilon_0\varepsilon_r D^2$ provides most of the Coulomb piece, $z - z'/D$ picks out the *z*-component,

Figure 21, and $\rho(r,z\,|\,z',i)\,d\vec{r}\,dz$ is the charge of mobile ions in a differential volume $d\vec{r}\,dz$.

Figure 21

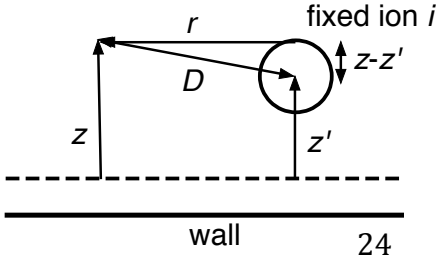

The other part of the mean force $f_i(z')$ is from the hard core repulsions. I'll write it down first, then explain it.

Eq. 51 $$f_i^{core}(z') = -k_B T \int \frac{z - z'}{a} c^{contact}(z \mid z', i)\, 2\pi a\, dz ,$$

where we have used the concentration of mobile ions in *contact* with the fixed ion *i*,

Eq. 52 $$c^{contact}(z \mid z', i) = c([a^2 - (z - z')^2]^{1/2}, z \mid z', i) ,$$

which is based upon an expression for the total concentration

Eq. 53 $$c(r, z \mid z', i) = \sum_j c_j(r, z \mid z', i) ,$$

for the case when $r = [a^2 - (z - z')^2]^{1/2}$, as shown in Figure 22 for a mobile ion in contact with the fixed ion *i*.

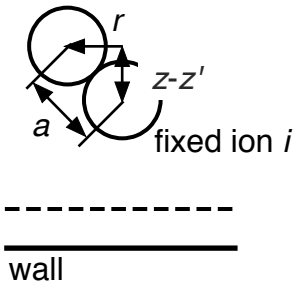

Figure 22

The force $f_i^{core}(z')$ is due to collisions by neighboring ions on the surface of the fixed ion *i*. The term $k_B T c^{contact}$ is a radial pressure, whereas $(z - z')/a$ selects the *z*-component of the pressure integrated over the spherical surface $2\pi a\, dz$ surrounding ion *i.* If $z > z'$, then $f_i^{core}(z') < 0$, but if $z < z'$, then $f_i^{core}(z') > 0$ (Figure 23). Positive forces are directed away from the wall.

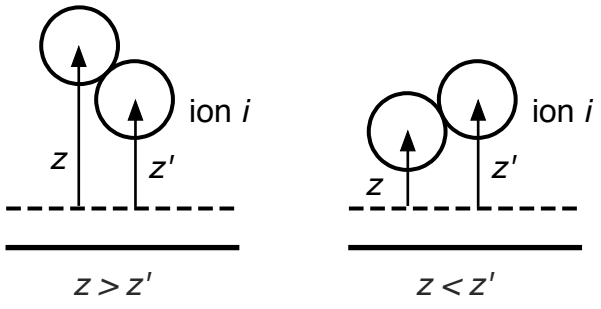

Figure 23

Aside on the derivation of Eq. 51:

From Eq. 39 and Eq. 46, we can write

$$f_i^{core}(z') = -\sum_j \int \frac{du_{ij}^{core}(D)}{dz'} c_j(\vec{R} \mid z', i)\, d\vec{R}.$$

The following equation can then be derived with the use of $g_{ij}(r,z,z') = \exp[-\beta u_{ij}^{core}(D)]\, y_{ij}(r,z,z')$, where y_{ij} is continuous across the hard core boundary and is identical to g_{ij} for $D > a$,

$f_i^{core}(z') = -k_B T \int \frac{z-z'}{a} \delta(D-a) \sum_j c_j(\vec{R} \mid z', i)\, d\vec{R}$, and $\delta(D-a)$ leads to contributions only from the contact concentration.

Mean Force and Potential of Mean Force in Poisson-Boltzmann Theory

Continuing to follow the development by Kjellander and Greberg (1998), we can make a useful comparison to the mean field Poisson-Boltzmann theory by rewriting Eq. 48 ($f_i(z') = f_i^{el}(z') + f_i^{core}(z')$). First, ions are point-like in Poisson-Boltzmann theory so that $f_i^{core,PB}(z') = 0$. Second, we replace $\rho(r,z \mid z',i)$ by the average charge density $\rho^{PB}(z)$ ($= \sum_j q_j\, c_j(z)$). Therefore, a modified version of Eq. 50 becomes the only contribution to the mean force on ion *i*.

Eq. 54 $$f_i^{PB}(z') = q_i \left[\frac{\sigma}{2\varepsilon_0 \varepsilon_r} - \int \frac{z-z'}{4\pi\varepsilon_0 \varepsilon_r D^3} \rho^{PB}(z)\, d\vec{r}\, dz \right],$$

where the quantity in brackets is just the mean electrostatic field acting on ion *i*, so that we can write

Eq. 55 $$f_i^{PB}(z') = -q_i \frac{d\phi^{PB}(z')}{dz'},$$

where $\phi^{PB}(z')$ is the mean electrostatic potential at the coordinate z'. The concentration profiles can then be calculated self-consistently using Eq. 54 and Eq. 55.

Since $f_i(z') = -dw_i(z')/dz'$ (Eq. 34), we can use Eq. 55 to write the potential of mean force for Poisson-Boltzmann theory,

Eq. 56 $$w_i^{PB}(z') = q_i \phi^{PB}(z') + \text{constant},$$

which leads to the well known expression for the ion concentration profile in P-B theory,

Eq. 57 $$c_i^{PB}(z') = c_i^{bulk} \exp[-\beta\, q_i \phi^{PB}(z')] .$$

To derive Eq. 57, we used Eq. 29 and chose the electrostatic potential in the bulk to be zero, $\phi^{PB,bulk} = 0$.

The approximations of P-B theory are equivalent to assuming that ion *i* fixed at z' does not affect the neighboring charge distribution – the ion is point-like and must have negligible charge for this to be true. Real ions behave differently because they have a substantial charge that repels like-charged ions and attracts opposite-charged ions. In addition, the finite ion size creates a cavity where no ions can enter and is responsible for collisional forces $f_i^{core}(z')$ that affect the ion distribution outside the cavity. Both the substantial charge of ion *i* as well as its finite size lead to a charge distribution $\rho(r, z \mid z', i)$ that is different from $\rho^{PB}(z)$.

Some Results

There are several different methods to use the theory developed in this section on many body effects to calculate ion concentration and charge density distributions, as well as the mean force or the potential of mean force. These include Monte Carlo computational methods and liquid state theories. The results of one liquid state theory, the reference hypernetted chain – RHNC – have been shown to be nearly quantitatively equivalent to those of Monte Carlo methods for the particular system outlined here. A detailed discussion of these methods is outside the realm of this short course, so I will just show you some graphical results to illuminate the roles that many body effects play in ion distributions. The results that I will discuss were presented previously in Kjellander and Greberg (1998).

These results will be calculated for a continuum solvent with the relative permittivity of water $\varepsilon_r = 78.7$ for either 1:1 electrolytes (cation with charge +1, anion with charge -1) or 2:2 electrolytes (cation with charge +2, anion with charge -2), where the former will be referred to as monovalent ions and the latter as divalent ions. The diameter, a = 4.25 Å, will be the same for all ions, the temperature T = 298 K, and the surface charge density, σ = –0.16 C m^{-2}, corresponds to 1 elementary charge per nm^2.

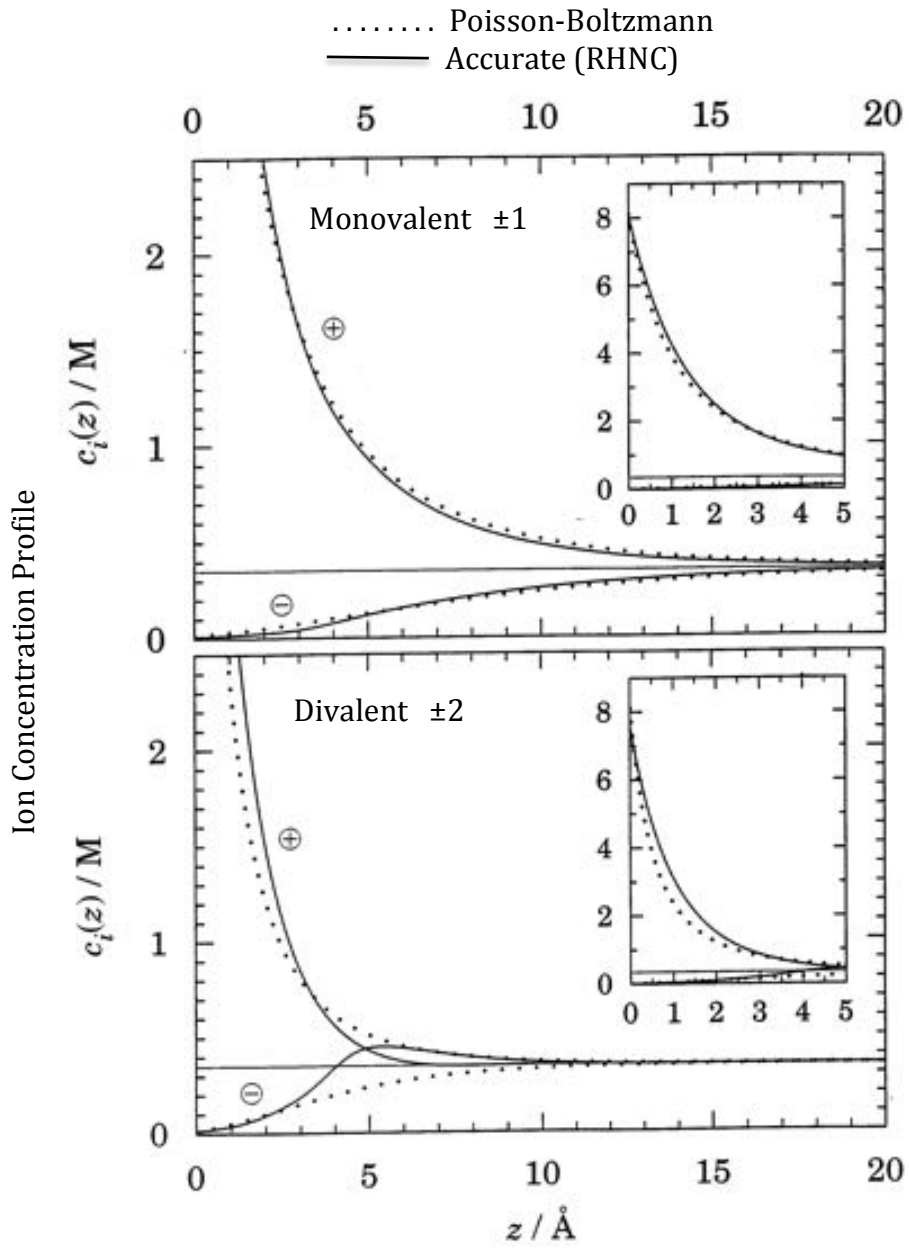

Figure 24 From Kjellander and Greberg (1998).

Monovalent ions – Poisson-Boltzmann and accurate profiles similar, though deviations are systematic and based upon simple physical ideas to be discussed. Asymmetry between + and – is the result of the negative charge of the wall. The coion (-) concentration is small and the counterion (+) concentration is large at the negatively charged wall.

Divalent - Poisson-Boltzmann and accurate profiles are qualitatively different for the coions (-2), which exhibit charge inversion for $z > 5$ Å for the accurate profile. In this region the charge density $\rho(z)$ is negative, the same as the wall. Accurate counterion (+2) concentration drops to bulk value much faster than for P-B.

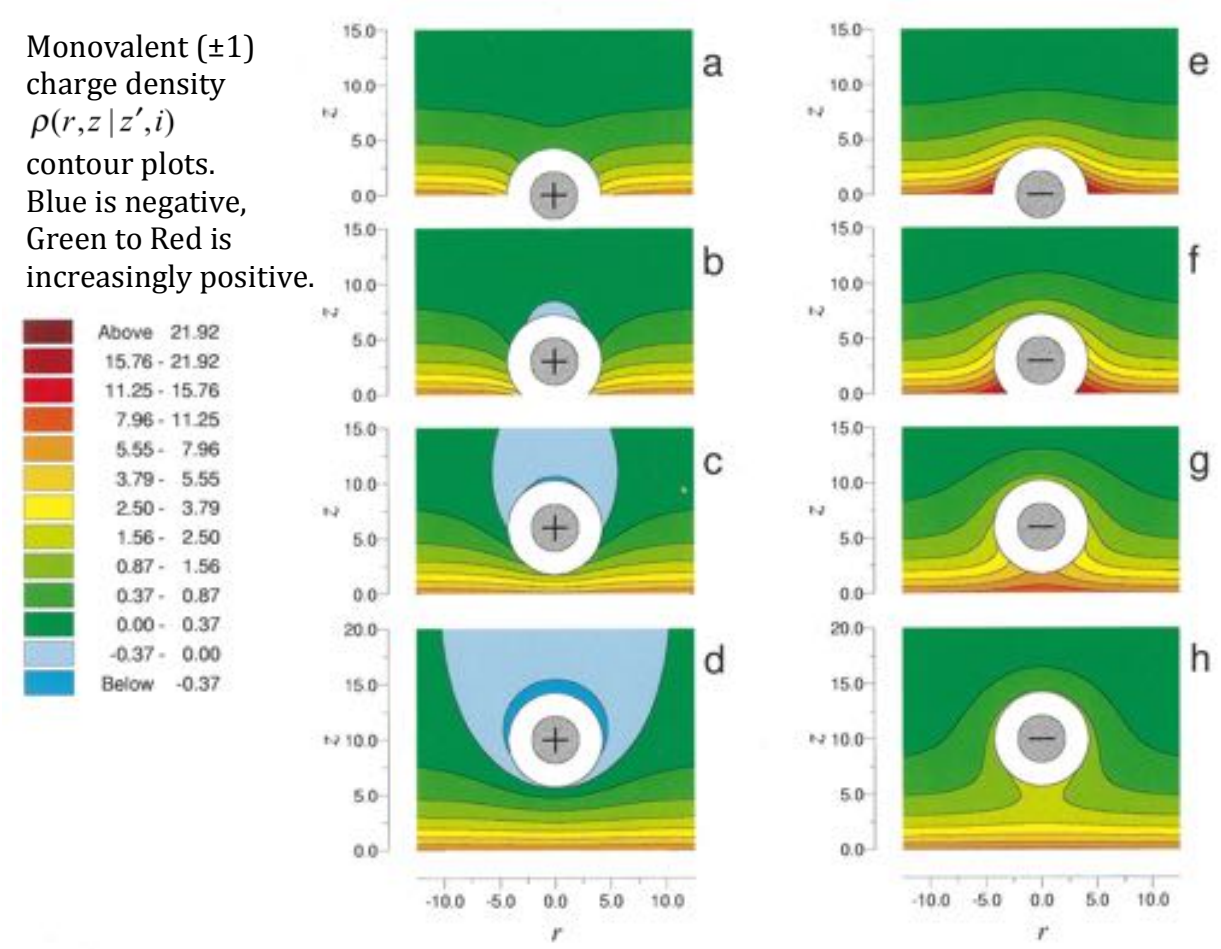

Figure 25 From Kjellander and Greberg (1998).

Grey circle – fixed ion *i* of diameter *a*.
White circle – excluded region of diameter 2*a* – centers of other ions cannot enter cavity.
(d) - Can observe nearly unperturbed charge density at large *r*.

(a–b) Relatively small perturbation due to +1 counterion at wall, which is due to a balance of two effects: (i)Coulomb repulsion of mostly counterions near the wall, and (ii) large number of collisions within the high density of mobile counterions at wall which push mobile counterions towards the fixed counterion.

(c-d) Counterion starts to attract coions as it moves away from the wall, where the coion density is larger.

(e-f) very large perturbation in attracting mobile counterions near the wall – Coulomb attraction of fixed coion with high density of mobile counterions near wall, plus core collision effect.

Divalent (±2)
charge density
$\rho(r,z\,|\,z',i)$
contour plots.
Blue is negative,
Green to Red to Purple
is increasingly positive.

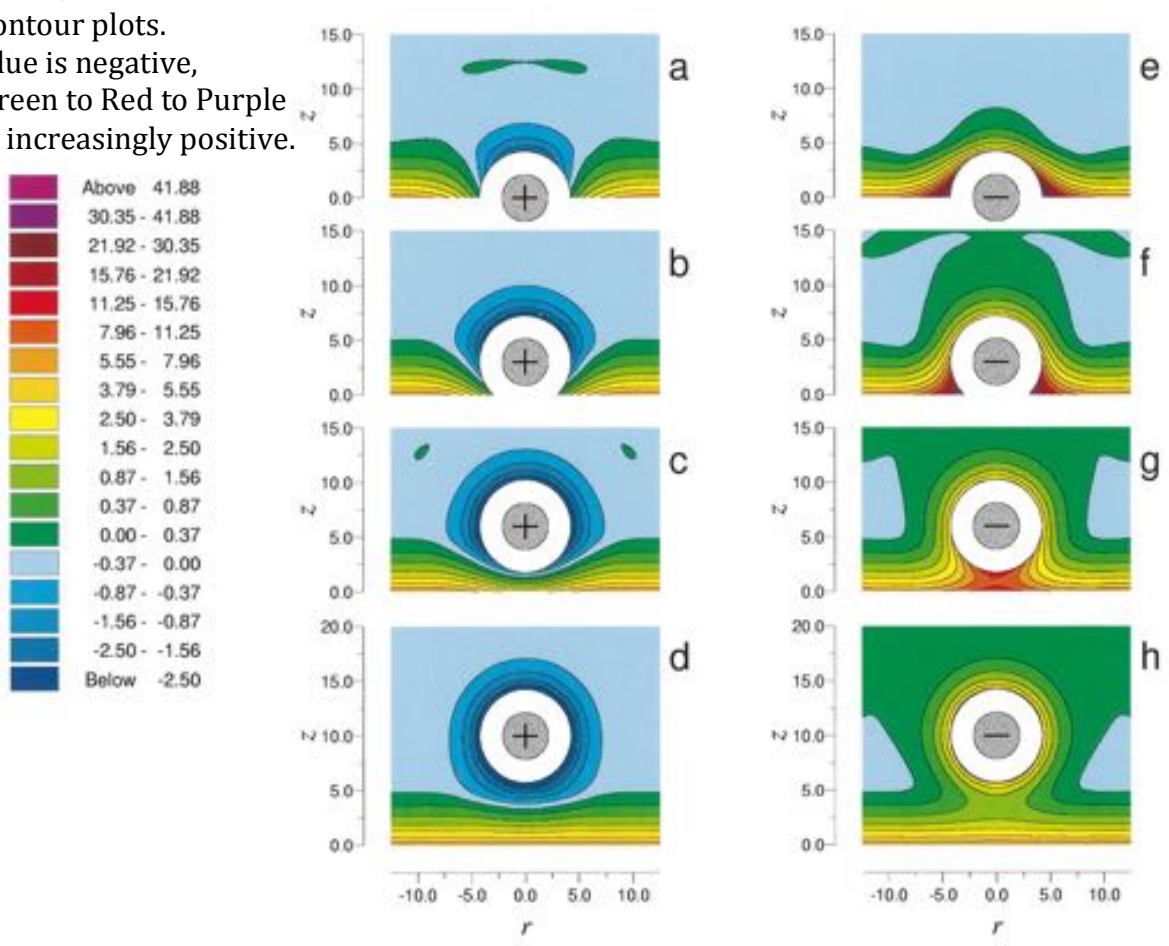

Figure 26 From Kjellander and Greberg (1998).

Much larger perturbation from divalent ions than for monovalent ions shown in Figure 25 due to the increase in Coulomb attraction by a factor of 4. (Note that a numerical comparison of charge densities requires multiplying those in Figure 26 by a factor of 2).

(d) Shift from green to blue at large in-plane r indicates charge inversion for $z > 5$ Å .

(a-b) Strong Coulomb attraction brings mobile coions to wall and repels high density of mobile counterions near wall. This effect is aided by the large coion concentration at about $z = 5$ Å, shown in Figure 24. Coulomb repulsion dominates core collisions that push mobile counterions at the wall towards the fixed counterion.

(e) Very large Coulomb attraction of high density of mobile counterions at wall.

Polarization effects

Figure 25 and Figure 26 show that the region in the neighborhood of the fixed ion is polarized (from both Coulomb and hard sphere effects). The polarization is particularly strong for the divalent ions illustrated in Figure 26. Here, we define a polarization charge density induced by the fixed ion as

Eq. 58
$$\rho^{pol}(r,z\,|\,z',i)=\begin{cases}\rho(r,z\,|\,z',i)-\rho(z) & D\geq a \quad \text{(outside cavity)}\\ 0 & D<a \quad \text{(inside cavity)}\end{cases}$$

Divalent (±2) polarization charge density $\rho^{pol}(r,z\,|\,z',i)$ contour plots.

Blue is negative,

Green to Red
to Purple
is increasingly positive.

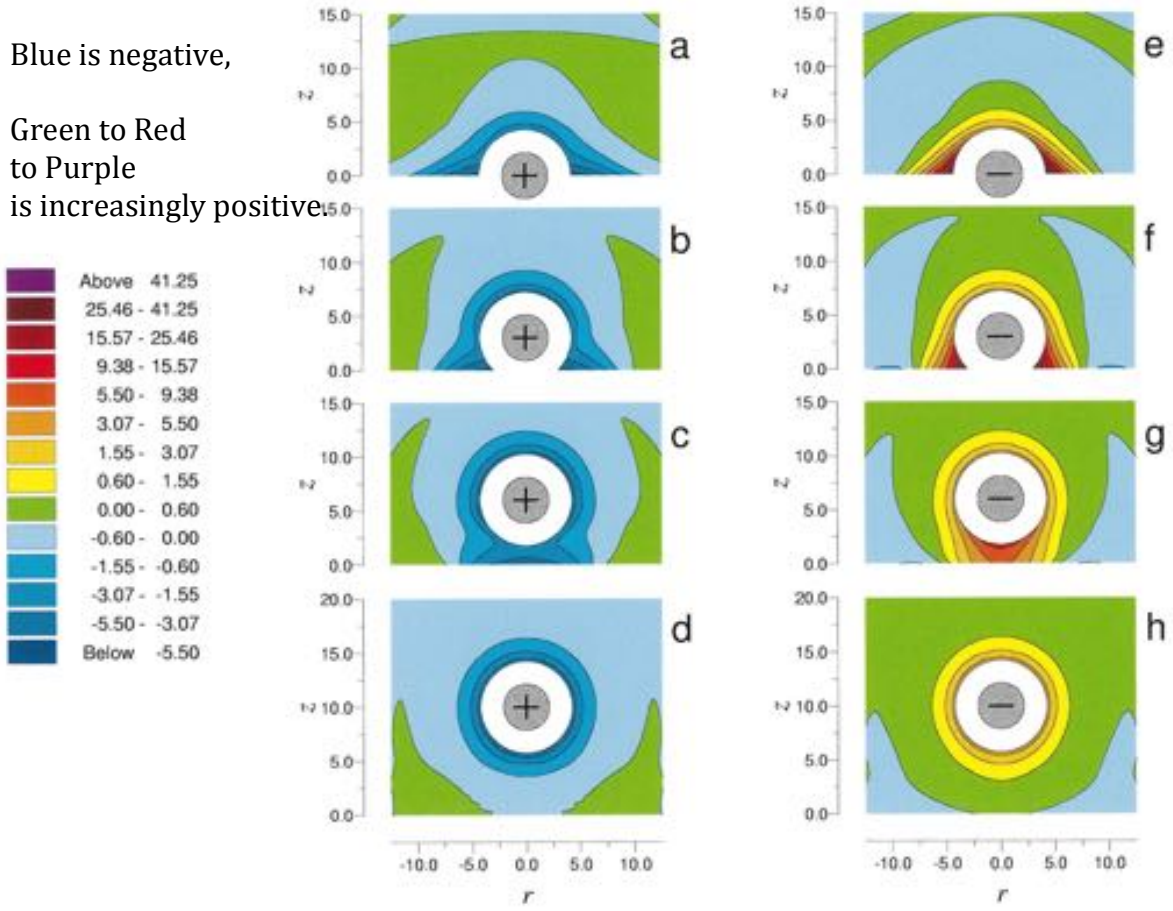

Figure 27 From Kjellander and Greberg (1998).

Having subtracted the average charge density, the much larger polarization from the fixed coion (-2) near the wall compared to the fixed counterion (+2) near the wall is evident. This difference is due primarily to the attraction of mobile counterions to the fixed coion versus the repulsion of mobile counterions to the fixed counterion because the ion density near the wall consists of almost exclusively mobile counterions. The asymmetry is the result of the non-linear behavior of the Boltzmann factor, which gets asymmetrically larger for a positive exponent compared to a negative exponent. Far from the wall where the ion profile consists of mobile coions and counterions, the differences are smaller.

Force Profiles

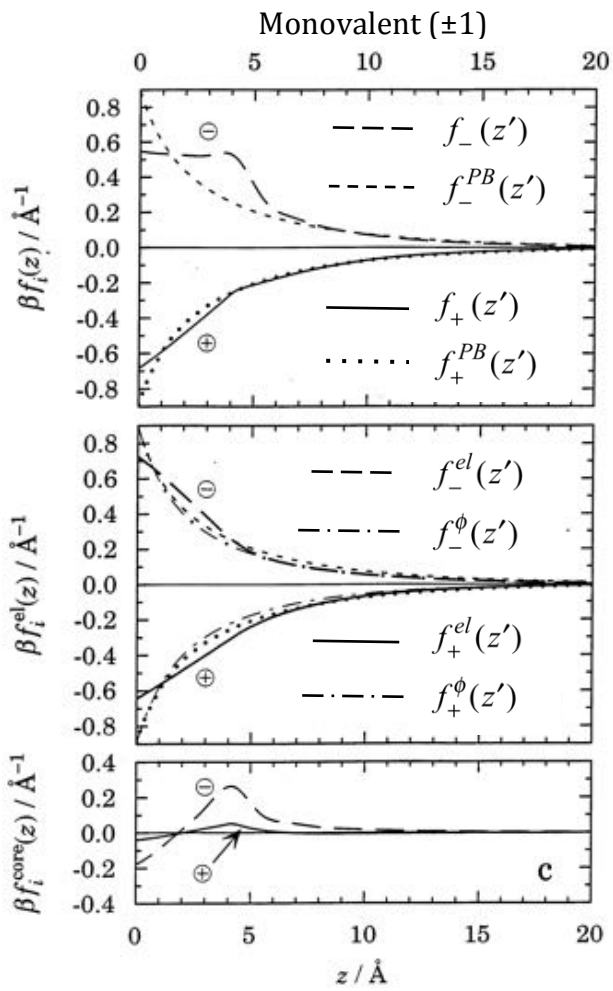

Figure 28 From Kjellander and Greberg (1998).

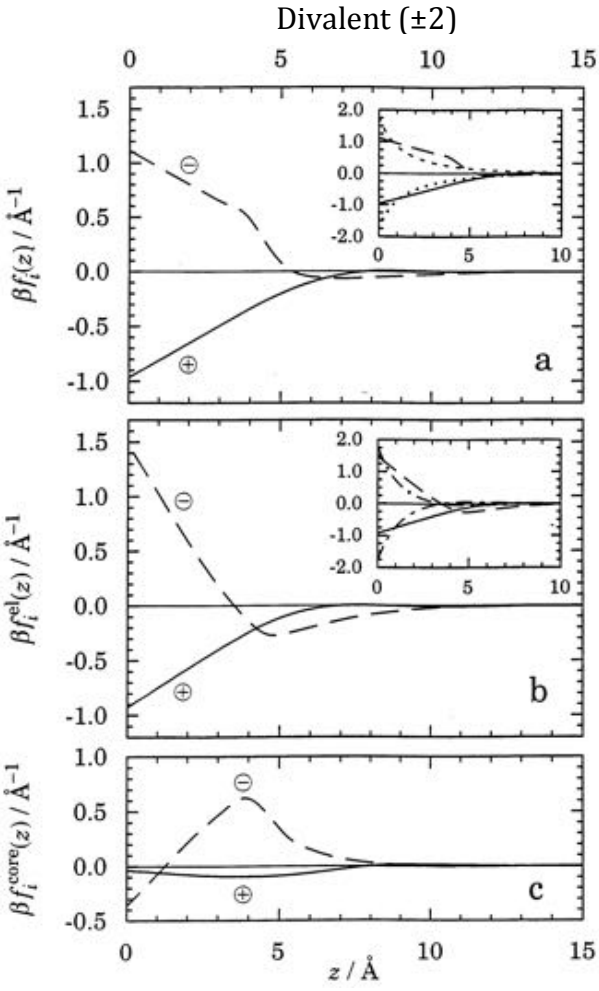

Figure 29 From Kjellander and Greberg (1998).

In Figure 28a and Figure 29a monovalent coions (–) are repelled and counterions (+) attracted for all z, but divalent coions are attracted for $z > 5$ Å, consistent with charge inversion of divalent ions.

In Figure 28c and Figure 29c core collisions provide a substantial force for $z < 5$ Å. When a fixed coion is in contact with the wall, mobile ions collide with its top half, pushing it into the wall and produce $f_i^{core}(z') < 0$.

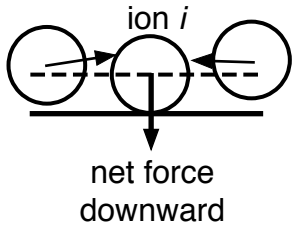

As the fixed coion is moved to larger z, mobile ions collide with the bottom half as well, but since the mobile ions are denser near the wall, the effect is to push the fixed ion

away from the wall, $f_i^{core}(z') > 0$. The Coulomb attraction of the predominant counterions near the wall for the fixed coion increases the counterion density and the number of collisions on the coion. The opposite happens for the fixed counterion, leading to a smaller effect as seen in Figure 28c.

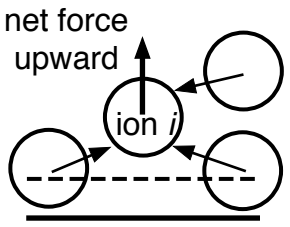

When the fixed ion is at higher *z*, it loses contact with the large concentration of ions closer to the wall, so that $f_i^{core}(z')$ decrease, though it remains positive since there are more mobile ions in contact with it on the side closer to the wall. Something different is happening in Figure 29c for counterions that will be discussed later.

In Figure 28a, the force from core collisions is the primary difference from the P-B theory for monovalent ions.

We'll return to these figures later. For now, let's address the relative importance of two contributions to the many body effects.

Cavity vs. Electrostatic Polarization Effects

The influence of a fixed ion on its neighboring ions is due to both hard core and electrostatic effects. Now, we will present some calculations that try to identify their relative importance. We will find that the cavity dominates the ion-induced polarization for monovalent ions, but that electrostatic effects dominate it for divalent ions.

Let's remind ourselves of the forces that we are considering, as well as define two more forces to help us distinguish between cavity and electrostatic effects.

Force	Expression	Eq. #	Description
$f_i^{el}(z')$	$= q_i \left[\frac{\sigma}{2\varepsilon_0\varepsilon_r} - \int \frac{z-z'}{4\pi\varepsilon_0\varepsilon_r D^3} \rho(r,z \mid z',i)\, d\vec{r}\, dz \right]$	Eq. 50	Electrostatic part of full force on fixed ion *i*
$f_i^{PB}(z')$	$= q_i \left[\frac{\sigma}{2\varepsilon_0\varepsilon_r} - \int \frac{z-z'}{4\pi\varepsilon_0\varepsilon_r D^3} \rho^{PB}(z)\, d\vec{r}\, dz \right]$	Eq. 54	Force due to average $\rho^{PB}(z)$
$f_i^{\phi}(z')$	$= q_i \left[\frac{\sigma}{2\varepsilon_0\varepsilon_r} - \int \frac{z-z'}{4\pi\varepsilon_0\varepsilon_r D^3} \rho(r)\, d\vec{r}\, dz \right]$	Eq. 59	Force due to average $\rho(z)$ from the full theory, but $\rho(z)$ is unperturbed by a fixed ion.
$f_i^{P-C}(z')$	$\frac{df_i^{P-C}(z')}{dz'} = \frac{q_i}{2\varepsilon_0\varepsilon_r a} \int_{z'-a}^{z'+a} \rho(z)\, dz$		(Profile – Cavity) force due to average $\rho(z)$ from the full theory, but minus the cavity (i.e., a hole of radius *a* cut out of $\rho(z)$). Similar to $f_i^{\phi}(z')$, but with cavity at fixed z'. Does not include polarization effects of $\rho(r,z \mid z',i)$.
$f_i^{core}(z')$	$= -k_B T \int \frac{z-z'}{a} c^{contact}(z \mid z',i)\, 2\pi a\, dz$	Eq. 51	Force due to core collisions (this is different from the electrostatic effect of the cavity)

Here, two new forces have been introduced. First, the force due to the average $\rho(z)$ from the full theory,

Eq. 59 $$f_i^{\phi}(z') = q_i \left[\frac{\sigma}{2\varepsilon_0\varepsilon_r} - \int \frac{z-z'}{4\pi\varepsilon_0\varepsilon_r D^3} \rho(r)\, d\vec{r}\, dz \right].$$

Note that $f_i^{\phi}(z')$ is different from $f_i^{PB}(z')$ because $f_i^{\phi}(z')$ includes the averaged effects of core collisions, the cavity, and the ion-induced polarization.

Second, the profile minus cavity force $f_i^{P-C}(z')$ is due to the average $\rho(z)$ from the full theory, but with a hole of radius *a* cut out of it. This is similar to $f_i^{\phi}(z')$, but with a cavity at fixed z'. Note that $f_i^{P-C}(z')$ does not include the polarization outside the cavity due to $\rho(r,z\,|\,z',i)$.

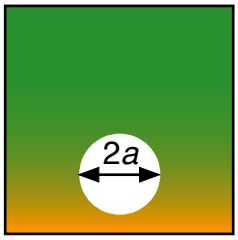

- Comparing $f_i^{el}(z')$ to $f_i^{\phi}(z')$ isolates the effect of a fixed ion perturbing its neighborhood, but cannot distinguish between effects caused by the cavity from those caused by polarization in the neighborhood of the fixed ion.
- Comparing $f_i^{\phi}(z')$ to $f_i^{P-C}(z')$ isolates the effect of the cavity.
- Comparing $f_i^{el}(z')$ to $f_i^{P-C}(z')$ provides insight into the ion-induced polarization.

Monovalent Ions

First, let's look back at Figure 28b, which shows very small differences between $f_i^{\phi}(z')$ and $f_i^{PB}(z')$. This is not unexpected because the concentration profiles are very similar in the monovalent case. However, small, but not insignificant differences are observed between $f_i^{el}(z')$ and $f_i^{\phi}(z')$, which show that either cavity effects or ion-induced polarization are important. To distinguish these two effects for monovalent ions, look at Figure 30. Since the $f_i^{el}(z')$ and $f_i^{P-C}(z')$ curves in Figure 30 are similar for monovalent ions, *the cavity is the dominant effect.*

The two forces for counterions (+) are almost the same, indicating that ion-induced polarization is small, as we saw in Figure 25a-d. A small effect of polarization is observed for coions (-). It may seem odd that the visible effects that were observed in Figure 25, lead to such small effects on the forces. This is a result of the fact that the forces provide only the net component in the *z*-direction.

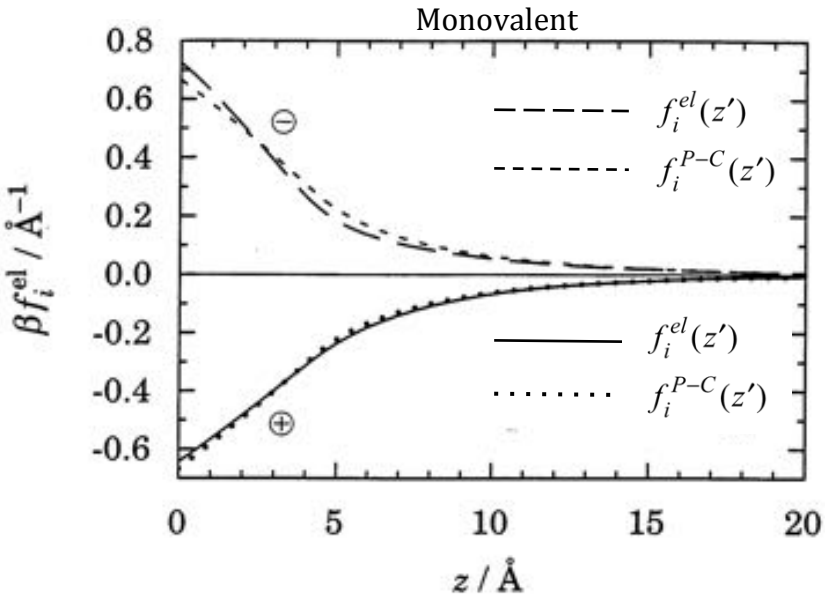

Figure 30 From Kjellander and Greberg (1998).

Now, let's think a little more about cavity effects. We are not referring to core collisional effects, but rather to the fact that the presence of a cavity excludes mobile ions from entering that region. In the Poisson-Boltzmann theory, ions are point-like and the "cavity" is filled with ions. This is also the case when we calculate $f_i^{\phi}(z')$.

Figure 31

Figure 28b shows that $f_-^{el}(z') > f_-^{\phi}(z')$ for $1 < z' < 4$ Å, which Figure 30 indicated is due to cavity effects. In this range, a fixed coion (–) might be situated as shown in Figure 31. If the ion cavity does not exclude mobile ions, also as shown in Figure 31, then more counterions (+, orange in the figure) are found between the fixed ion charge (located at the ion center in this theory) and the negatively charged wall. These counterions in the volume otherwise occupied by the cavity shield the negative charge of the wall from the fixed ion and reduce the repulsive force of the wall on the fixed ion. Therefore $f_-^{el}(z') > f_-^{\phi}(z')$.

A similar shielding effect will occur for a fixed counterion (+), for which the attraction to the wall will be reduced if there are mobile counterions in the cavity, which should not be there. This also leads to $\left|f_+^{el}(z')\right| > \left|f_+^{\phi}(z')\right|$, but now both forces are negative.

Very close to the wall, $z' < 1$ Å , the cavity effect reverses sign. In this case, Figure 32 shows that most of the extra mobile counterions in the cavity are on the opposite side of the ion center, leading to an additional repulsive (positive) force. Now $\left|f_i^{el}(z')\right| < \left|f_i^{\phi}(z')\right|$ for $z' < 1$ Å .

Figure 32

These statements hold true for Poisson-Boltzmann theory, which means that very close to the wall – when ions are nearly in contact with the wall, $z' < 1$ Å – the wall is inadequately shielded and there are too many counterions and not enough coions. The contact density at the wall is too high. This is a well-known problem that produces Poisson-Boltzmann predictions for the contact ion density that can even exceed the space available to put the ions.

At intermediate distances, $1 < z' < 4$ Å , Poisson-Boltzmann theory produces a wall that is too well shielded, leading to too few counterions and too many coions. This leads to a net shielding of the wall charge that is too small and positively charged particles further from the wall, $z' > 4$ Å , will be too strongly attracted and negatively charged particles too strongly repelled. This effect is visible in Figure 24 for monovalent counter- and coions, but even more so for divalent counterions.

Divalent Ions – Charge Inversion

We have observed that effects observed for monovalent ions, perhaps weakly, become stronger for divalent ions because of the increase in Coulomb interactions by a factor of 4. The effects of the cavity that we have just discussed are present for divalent ions, but we will see that the effects of ion-induced polarization dominate the cavity effects in determining $f_i^{el}(z')$.

An important new observation for divalent ions is the presence of charge inversion that appeared for divalent ions in Figure 24 for $z' > 5$ Å . This corresponds to the total mean force becoming negative, $f_-(z') < 0$, for $z' > 5$ Å as shown in Figure 29a. Figure 29b&c shows that this occurs because $f_-^{el}(z')$ is more negative than $f_-^{core}(z')$ is negative in this region.

The large excess of mobile counterions between the fixed coion and the wall observed in Figure 26f-h leads to a large attraction of the coion for the wall. Figure 33 shows that $f_-^{el}(z')$ provides a large attraction that dominates the effect of $f_i^{P-C}(z')$ for

$z' > 5$ Å , unlike the monovalent case for which the two forces were similar. This shows the importance of the ion-induced polarization that is not included in $f_i^{P-C}(z')$. This is also consistent with the large polarization charge density of counterions shown in Figure 27f-g that exist between the fixed coion (–) and the wall.

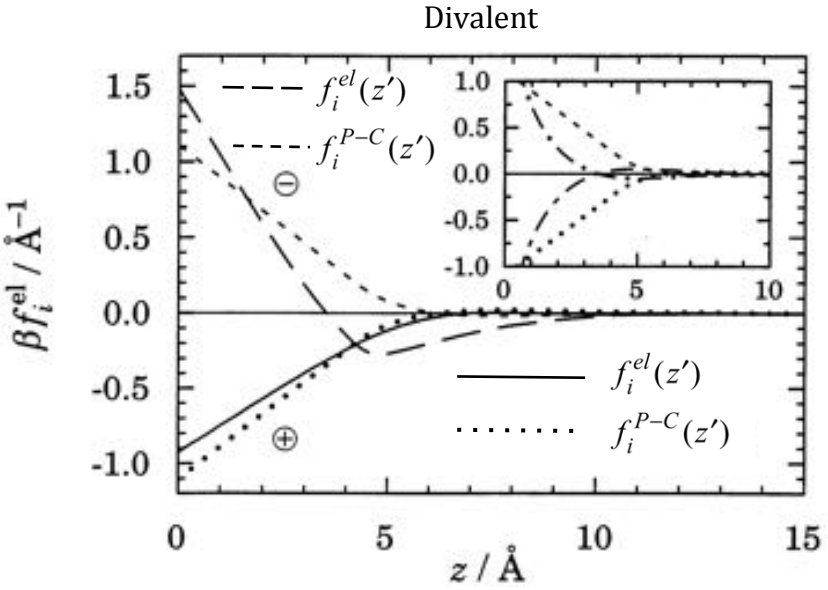

Figure 33 From Kjellander and Greberg (1998).

Polarization effects attract both mobile coions and counterions in this intermediate region from the wall, but the effect is much greater for coions because of the non-linear Boltzmann factor. At short distances from the wall, the polarization effects are reversed because there is not much room for mobile ions between the fixed ion and the wall.

Charge Reversal Another effect related to the charge inversion of coions is charge reversal of the surface, which occurs when the net counterion charge within a few angstroms of the surface, say $z' < 5$ Å exceeds the net surface charge. In this case, the overcompensation of the negative surface charge by positive counterions leads to a reversal of the effective net charge of the surface. This must happen, in order to preserve charge neutrality, if there is charge inversion of coions. However, in some cases, though not the one illustrated here, charge reversal of the surface can be the dominant cause of charge inversion.

Charge reversal is the result of large numbers of counterions at the wall, which result from both electrostatic interactions previously described and core collisions. Core collisions attract a positive fixed counterion to the wall because there is a lower density of mobile counterions between it and the wall as a result of repulsive forces (Coulombic and hard core repulsions). This is sometimes called a “correlation hole” that exposes the wall charge. In addition, attraction of coions on the side of the fixed counterion away from the wall leads to more collisions on the side of the fixed ion further from the wall than on its side closer to the wall, which results in a collision force on the counterion towards the wall.

The larger Coulomb forces present with divalent ions enhance this effect over the case of monovalent ions.

Summary Comparison for Monovalent and Divalent Ions

In this section on many body effects in the primitive model, we have observed that the primary factors that distinguish accurate theory from Poisson-Boltzmann theory for monovalent ions are the ion cavity and, for coions, the core collision force. The main effect of the ion cavity for ions at intermediate distances from the wall is to reduce the shielding of the wall charge by mobile counterions. This leads to greater attraction of counterions to the wall and greater repulsion of coions from the wall. Right at the wall, for $z' < 1$ Å , the opposite effect occurs, which lowers the contact concentration of counterions at the wall from the Poisson-Boltzmann value. This reduction in contact concentration, $c(0)$, can have a significant effect on the pressure, given by the contact theorem as

Eq. 60 $$P = k_B T\, c(0) - \frac{\sigma^2}{2\varepsilon_0 \varepsilon_r}$$

because the two terms on the right hand side often have very similar magnitudes.

Contrary to the case of monovalent ions, the larger Coulomb interactions of divalent ions lead to strong polarization that produce effects such as charge inversion and charge reversal that are qualitatively different from effects produced by Poisson-Boltzmann theory. In P-B theory, ion concentration profiles either monotonically increase (for coions) or decrease (for counterions) when moving away from the wall. Charge inversion means that the profiles are non-monotonic. In addition, Poisson-Boltzmann theory predicts that counterions shield a charged wall by reducing its effective charge observed away from the wall. However, the many-body effects described above can lead to overcompensation of the wall charge by the counterion charge close to the wall. This effectively reverses the apparent charge of the wall observed 5 to 10 Å away from the wall.

Note that these observations are for the specific model chosen. For example, charge inversion can occur in monovalent systems if the counterions are smaller than the coions. Once again, cavity effects will dominate for monovalent ions and the different sizes will play a role.

A Model System for Soft Interfaces

Up till now, we have discussed a hard surface in contact with an electrolyte solution. Now I'd like to introduce a model system for a soft interface, the liquid-liquid interface between two immiscible electrolyte solutions.

Liquid-Liquid Interfaces

Many organic liquids form phase separated bi-phase systems when placed in contact with water, like oil and water. Some organic liquids have a large relative permittivity that allows organic-soluble electrolytes to dissociate upon being dissolved in the organic liquid. For example, 1,2-dichlorethane has a relative permittivity $\varepsilon_r = 10.4$, and nitrobenzene has $\varepsilon_r = 34.8$. You can have in mind the system in Figure 34 (minus the nanoparticle at the interface, of course!).

The liquid-liquid interface in neat water-organic biphase liquid systems, where "neat" means that there are no additives like electrolytes or surfactants, has been measured by x-ray scattering to be molecularly sharp with intrinsic structure on the order of 1 Å, which is smaller than the molecules themselves. In other words, in spite of a small solubility of one component in the other, say a percent or so, the interface is not a region where molecules from the two phases are substantially mixed. However, these soft interfaces have fluctuations driven by thermal energy – fluctuations known as capillary waves. These waves have amplitudes on the order of a few angstroms (~4 Å overall for the neat DCE/water interface, for example), and wavelengths that vary from close to the molecular size to the size of the sample. A thorough discussion of this aspect of liquid interfaces can be found in a recent book that describes x-ray scattering from liquid surfaces, including the effect of capillary waves (Pershan and Schlossman 2012).

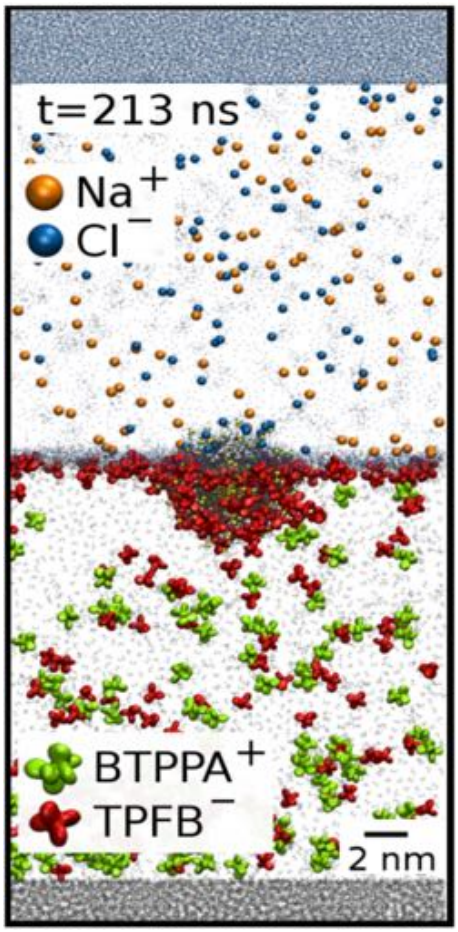

Water phase

Organic phase (1,2-dichloroethane, abbreviated DCE)

Figure 34 From (Bera et al. 2014).

In addition to a slight miscibility of the solvents (say, 1% water in DCE and vice versa), there is a possibility that the ions can be partially soluble in both liquid phases. In this case, the ions can partition between the two liquid phases and set up an electrostatic potential difference between them.

Prior to discussing this effect, let's just briefly review chemical potentials, using the electrochemist's conventional notation. In this case the chemical potential μ_i is the work done to transfer a mole of species *i* from the vacuum to a phase, minus the work of volume expansion, and can be written in terms of the Gibbs free energy *G* and the number of moles, n_i, of species *i*,

Eq. 61 $$\mu_i = \left(\frac{\partial G}{\partial n_i} \right)_{T,p,n_{j \neq i}},$$

where the temperature, pressure and number of other species are kept constant. It can be shown that the chemical potential for a solute *B* in a solvent *A* can be written as

Eq. 62 $$\mu_B = \mu_B^{\circ} + RT \ln x_B + RT \ln \gamma_B = \mu_B^{\circ} + RT \ln a_B ,$$

where $\mu_B = \mu_B^{\circ} + RT \ln x_B$ is the chemical potential of an ideal solution (no interactions between the solutes) with μ_B° being the chemical potential with respect to a reference state (such as a state of infinite dilution), x_B is the molar fraction of solute *B*, *R* is the gas constant and $RT \ln x_B$ is the configuration mixing entropy due to the different ways of rearranging the solute B. The term $RT \ln \gamma_B$ is a fudge factor that accounts for non-idealities of the solution (i.e., interactions between the *B* solutes), where γ_B is called the activity coefficient. The last term contains the activity $a_B = \gamma_B x_B$. In equilibrium, μ_B is constant throughout the solution.

In the case of electrolyte solutions it is conventional to write

Eq. 63 $$\tilde{\mu}_i = \mu_i^{\circ} + RT \ln a_i + Z_i F \phi ,$$

where the last term is the electrostatic energy to move a mole of ions of charge Z_i from vacuum, where $\phi = 0$, to within the bulk of the liquid phase that has a constant value of the electrostatic potential ϕ (which we have previously called ϕ^{bulk}). Within the context of discussing moles of ions, the Faraday constant *F* is 96,485 coulombs per mole of monovalent ions.

The so-called electrochemical potential $\tilde{\mu}$ is just a chemical potential, but for charged solutions, and is constant throughout the solution.

Now, let's return to the description of two electrolyte solutions in thermodynamic equilibrium with each other and allow for the possibility that ions can transfer between the two phases. The standard Gibbs transfer energy is defined as the difference between the standard chemical potential for ion *i* in the two phases,

Eq. 64 $$\Delta G_{tr,i}^{\circ,\,\mathrm{wat}\rightarrow\mathrm{org}} = \mu_i^{\circ,\,\mathrm{org}} - \mu_i^{\circ,\,\mathrm{wat}}$$

If, for example, $\mu_i^{\circ,\,\mathrm{wat}} < \mu_i^{\circ,\,\mathrm{org}}$, as would be true for Na^+ in the case of water and DCE, then $\Delta G_{tr,i}^{\circ,\,\mathrm{wat}\rightarrow\mathrm{org}} > 0$ to transfer Na^+ from water to DCE and it would be unfavorable to do so.

Equating the electrochemical potentials for species *i* in the two phases,

Eq. 65 $$\mu_i^{\circ,\,\mathrm{wat}} + RT \ln a_i^{\mathrm{wat}} + Z_i F \phi^{\mathrm{wat}} = \mu_i^{\circ,\,\mathrm{org}} + RT \ln a_i^{\mathrm{org}} + Z_i F \phi^{\mathrm{org}} ,$$

allows us to write the difference in the electrostatic potential between the water and organic phases in terms of the activities (proportional to the concentrations) of species *i* in each phase,

Eq. 66 $$\Delta\phi^{\text{w-o}} = \phi^{\text{wat}} - \phi^{\text{org}} = \frac{\Delta G_{tr,i}^{\text{o, wat}\rightarrow\text{org}}}{Z_i F} + \frac{RT}{Z_i F}\ln\left(\frac{a_i^{\text{org}}}{a_i^{\text{wat}}}\right)$$

Eq. 66 is known as a Nernst equation. The so-called common ion technique takes advantage of the dependence of $\Delta\phi^{\text{w-o}}$ on concentration by dissolving A^+B^- in water and A^+C^- in the organic phase, for which the ion A^+ has substantial solubility in both phases, see Figure 35. Varying the initial concentration of, say A^+B^- in water, before putting the two phases in contact, allows the electrostatic potential difference between the two phases $\Delta\phi^{\text{w-o}}$ to be varied.

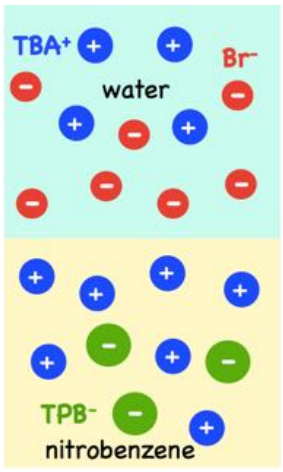

Figure 35

The type of electrified liquid-liquid interface that I have just described is referred to as *unpolarizable* because if we placed electrodes in the two phases and connected a voltage source across them, ions would repartition between the two phases by transporting across the liquid-liquid interface.

Alternatively if the standard Gibbs transfer energy for an ion is large, then it has a strong preference for one phase. For example, if A^+B^- is soluble in water and nearly insoluble in the organic phase, and C^+D^- is soluble in the organic phase, but nearly insoluble in water, then we can impose a potential difference across the two phases without substantial transfer of ions across the interface. An *ideally polarizable* liquid-liquid interface would not have any ion transfer. Instead, when a potential difference is imposed between the two liquid phases, excess charge builds up on either side of the liquid-liquid interface, leading to back-to-back electrical double layers at this interface, as illustrated in Figure 36. Placing metal electrodes into the two phases and using a voltage source allows the electrostatic potential difference $\Delta\phi^{\text{w-o}}$ between the two phases to be varied.

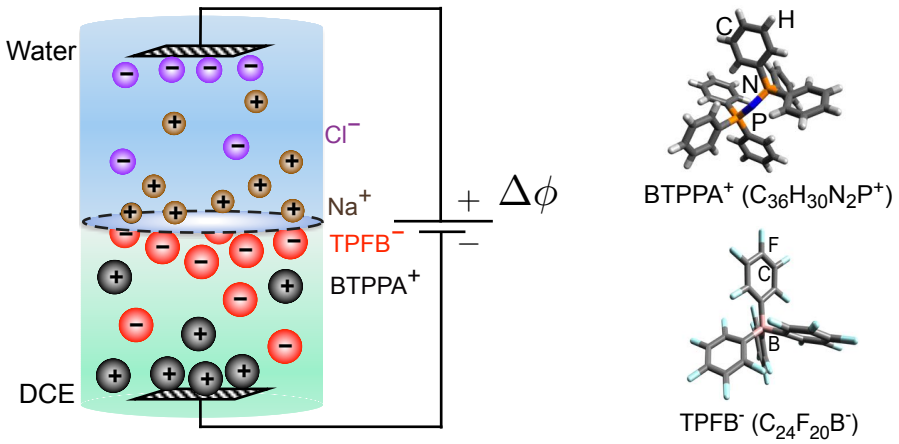

Figure 36

Varying the electrostatic potential difference $\Delta\phi^{\text{w-o}}$ changes the interfacial excess of ions. This changes the interfacial tension, which can be measured as shown in Figure 37.

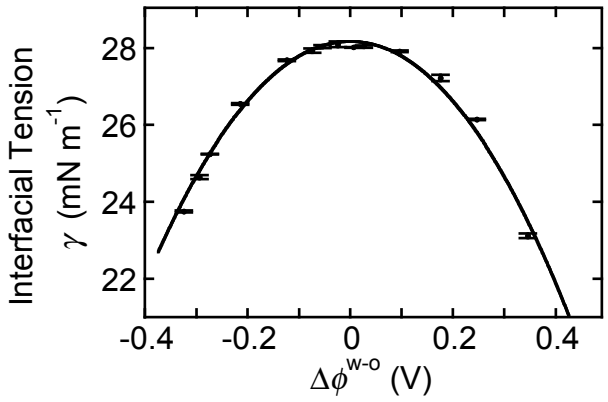

Figure 37 Interfacial tension from the water (10 mM NaCl) – DCE (5 mM BTPPATPFB) liquid-liquid interface, from (Hou et al. 2013).

The interfacial excess charge per unit area $Q_{tot}(\Delta\phi^{w-o})$ as a function of electric potential difference $\Delta\phi^{w-o}$ is determined by the variation of interfacial tension γ with $\Delta\phi^{w-o}$,

Eq. 67 $$Q_{tot}(\Delta\phi^{w-o}) = -(\partial\gamma / \partial\Delta\phi^{w-o})_{T,p,\mu_i}$$

Knowledge of the ion distributions can also yield the interfacial excess charge, which can be obtained by integrating the product of ion concentration $c_i(\Delta\phi^{w-o}, z)$ and ion charge $Z_i e$, summed over all types *i* of ions in the sample, from the interface into the bulk liquid far enough from the interface so that the ion concentrations have attained their bulk values,

Eq. 68 $$Q_{tot}(\Delta\phi^{w-o}) = \sum_i \int_{z=0}^{bulk} Z_i e\, c_i(\Delta\phi^{w-o}, z)\, dz$$

The magnitude of $Q_{tot}(\Delta\phi^{w-o})$ is independent of the bulk phase, but will have opposite sign for the water or DCE phase for a given value of $\Delta\phi^{w-o}$. The sign convention implicit in Eq. 67 yields $Q_{tot}(\Delta\phi^{w-o})$ on the water side of the interface.

The apex of the electrocapillary curve shown in Figure 37 corresponds to the condition $Q_{tot}(\Delta\phi^{w-o}) = 0$, which is known as the potential of zero charge, or pzc. At this potential the concentrations $c_i(\Delta\phi^{w-o}, z)$ are constant as *z* varies from the interface into the bulk liquids. It is conventional to assign the value of $\Delta\phi^{w-o}$ that makes $Q_{tot}(\Delta\phi^{w-o}) = 0$ to be $\Delta\phi^{w-o} = 0$, though this requires some justification (Girault and Schiffrin 1986).

What's Next?

At this point, we have discussed the mean-field Poisson-Boltzmann theory, some experimental phenomena that illustrate successes and failures of P-B theory, as well as a detailed discussion of the theoretical shortcomings of P-B theory. The shortcomings were highlighted within the context of the primitive model for liquids, which itself is an approximation to real systems which will fail to reproduce their behavior when the molecular structure of the solvent is important. Molecular structure is important when describing nanoscopic phenomena or soft interfaces whose structure, even without the electrostatic effects, depends upon the arrangement of molecules that can be easily perturbed.

At this time, there is not a universally accepted formalism for describing electrostatics at soft interfaces, and major challenges remain in this area (French et al. 2010), although there are several promising routes that include the many body effects previously discussed. These include liquid state integral equation theories, which have shown success at describing ion distributions at hard interfaces. Strong-coupling models of ion correlations in a classical Coulomb fluid have been studied, starting with Rouzina and Bloomfeld, including low-temperature models of Wigner crystallization of ions by Shklovskii and co-workers, and field theoretic approaches from Netz and others.

Many of these developments of analytic theory are tested against Monte Carlo calculations, so why not just use Monte Carlo or Molecular Dynamics simulations to predict the behavior of ions at interfaces? The complications of describing electrostatics near interfaces in soft systems remain challenging for computer simulations as well, partially because of the molecular complexity of the systems as well as for the multiple length scales that can be important. These include the short length scale of ion-molecule interactions, the structural length scale of the interface, the longer scale of the Debye length or the extent of electrostatic interactions, as well as the length scale of aggregated structures such as micelles or nanoparticles.

Here, we will be content to outline the use of density functional theory to describe electrostatics at interfaces and relate these results to some recent experiments. At the least, density functional theory provides more insight into Poisson-Boltzmann theory, but it also provides a way to include the molecular structure of the solvent and the interface, as well as a way to include many body effects such as ion correlations. This sounds promising, but as you will see, we will need to write a hybrid description that incorporates computer simulations and liquid state theory in a density functional framework. This hodge-podge may not be attractive, but it appears to describe experimental results.

Density Functional Theory

Density functional theory is designed to treat inhomogeneous systems. In our case, the inhomogeneities are due to an electrified interface or charged surface, which produces a spatial variation of the charge density $\rho(\vec{r})$ or ion concentration (density) distributions $c_{\pm}(\vec{r})$. Density functional theory has wide applicability in soft matter physics. The basic theory, along with a number of applications including Poisson-Boltzmann theory, are nicely reviewed in a book by Barrat and Hansen (2003). Let's first review the basic idea of density functional theory according to their presentation.

If the cause of the density inhomogeneity $\rho(\vec{r})$ can be written as an external potential, $V_{ext}(\vec{r})$, then it can be shown that

Eq. 69 $$\rho(\vec{r}) = -\frac{\delta \mathbf{\Omega}[\psi(\vec{r})]}{\delta V_{ext}(\vec{r})},$$

where the thermodynamic grand potential $\mathbf{\Omega}[\psi(\vec{r})]$ is a functional of the function $\psi(\vec{r}) = \mu - V_{ext}(\vec{r})$ consisting of the chemical potential μ and the external potential. Note that the derivative in Eq. 69 is a functional derivative, just like that used in the Euler-Lagrange equation (that expresses the principle of least action). Analogous to the Legendre transformation, $\mathbf{\Omega}(T,V,\mu) = F(T,V,N) - \mu N$, in conventional thermodynamics that allows the grand potential to be written in terms of the Helmholtz free energy, we can rewrite $\mathbf{\Omega}[\psi(\vec{r})]$ in terms of the Helmholtz free energy as a function of $\rho(\vec{r})$,

Eq. 70 $$\mathbf{\Omega}[\psi(\vec{r})] = F[\rho(\vec{r})] - \int \rho(\vec{r})\psi(\vec{r})d\vec{r}\,.$$

The free energy $F[\rho(\vec{r})]$ is a functional of $\rho(\vec{r})$, without explicit dependence on $\psi(\vec{r})$, and is, therefore, a property of the liquid or electrolyte solution. It can be proven that there is a unique relationship between $V_{ext}(\vec{r})$ and $\rho(\vec{r})$, and that

Eq. 71 $$\left.\frac{\delta \mathbf{\Omega}[\psi(\vec{r})]}{\delta \rho(\vec{r})}\right|_{\rho(\vec{r})=\rho_{eq}(\vec{r})} = 0,$$

which provides a method to find the equilibrium density variation $\rho_{eq}(\vec{r})$ by taking the functional derivative of Eq. 70 as follows,

Eq. 72 $$\frac{\delta}{\delta \rho(\vec{r})}\left(F[\rho(\vec{r})] - \int \rho(\vec{r})\psi(\vec{r})d\vec{r}\right)\Bigg|_{\rho(\vec{r})=\rho_{eq}(\vec{r})} = \left.\frac{\delta F[\rho(\vec{r})]}{\delta \rho(\vec{r})}\right|_{\rho(\vec{r})=\rho_{eq}(\vec{r})} + V_{ext}(\vec{r}) - \mu = 0\,.$$

The trick in applying density functional theory is to find an expression for $F[\rho(\vec{r})]$, which is known exactly only for the ideal gas,

Eq. 73 $$F_{\mathrm{id}}[\rho(\vec{r})] = k_B T \int \rho(\vec{r})[\ln(\rho(\vec{r})\Lambda^3) - 1]\, d\vec{r}\,,$$

which may remind you of the expression for a 1-component uniform ideal gas,

Eq. 74 $$F_{\mathrm{id}} = k_B T\, N[\ln(\rho\Lambda^3) - 1]\,,$$

where N is the number of particles and $\Lambda = h/\sqrt{2\pi m k_B T}$ is the de Broglie thermal wavelength for particles of mass m, and h is Planck's constant.

Poisson-Boltzmann Theory

The Poisson-Boltzmann equation can be derived from the density functional given by

Eq. 75 $$\frac{\beta}{A}\Omega^{PB}[c_{\pm}(z)] = \sum_{\pm}\left(\frac{\beta}{A}F^{PB}[c_i(z)] - \beta\int c_i(z)\mu_i\, dz\right),$$

where A is the surface or interfacial area, the concentration function $c_i(z)$ is the density of ion i, and μ_i is the chemical potential of ion i. The Poisson-Boltzmann free energy functional $F^{PB}[c_i(z)]$ is the sum of the ideal gas free energy in Eq. 73 and Coulomb interactions with a mean field $\phi(z)$,

Eq. 76 $$\frac{\beta}{A}F^{PB}[c_{\pm}(z)] = \int c_{\pm}(z)[\ln(c_{\pm}(z)\Lambda^3) - 1]\, dz \pm \frac{\beta}{2} e\int c_{\pm}(z)\phi(z)\, dz$$

This expression has been written for 1:1 electrolytes, but it could be easily modified for $Z_+ : Z_-$ electrolytes by multiplying the elementary charge e by $Z_{\pm}$. In this section and the next I am following a development described in more detail in my student's thesis (Laanait 2013). Note that the electrostatic potential $\phi(z)$ is a solution of Poisson's equation for the charge density $\rho(z) = e\left[c_+(z) - c_-(z)\right]$. It can be shown that the functional derivative of the grand potential is given by

Eq. 77 $$\frac{\beta}{A}\frac{\delta\Omega[c_{\pm}(z)]}{\delta c_{\pm}(z)} = \ln[(c_{\pm}(z)\Lambda^3] \pm \beta e\phi(z) - \beta\mu_{\pm}$$

Setting this functional derivative equal to zero, as in Eq. 71, yields an expression for the equilibrium values of the functions $c_{\pm}(z)$,

Eq. 78 $$c_{\pm}(z) = \Lambda^{-3}\exp[\beta\mu_{\pm} \mp \beta e\phi(z)]$$

As previously described, the Poisson-Boltzmann theory assumes that individual ions do not affect the neighboring charge distribution, allowing us to approximate the chemical

potential as that of an ideal solution, $\mu_{\pm} = k_B T \ln(c_{\pm}^{bulk} \Lambda^3)$, where the bulk concentrations $c_{\pm}^{bulk}$ are the same for monovalent ions. This leads to the standard expression for the Boltzmann distribution

Eq. 79 $$c_{\pm}(z) = c_{\pm}^{bulk} \exp\left[\mp e\phi(z) / k_B T\right],$$

which subsequently can be substituted into Poisson's equation to yield the Poisson-Boltzmann equation that we have already discussed.

This seems like a lot of work to just re-derive the P-B equation. It does, however, help to clarify the elements that go into its derivation: the entropy of an ideal gas of ions and the energy of mean field Coulomb interactions between ions. The derivation I presented did not properly clarify the role of the mean field. For those interested in this, see Barrat and Hansen (2003). Importantly, it also provides a way forward to include other aspects that determine ion distributions, though in an approximate way. These include the molecular structure of the solvent, ion-solvent interactions, and ion-ion correlations.

Returning to our discussion of the potential of mean force, Eq. 29 ($c_i(z') = c_i^{bulk} \exp[-\beta\,(w_i(z') - w_i^{bulk})]$) reminds us that we need to find an expression for the potential of mean force to place in the exponent. In the next two sections, we will write a density functional that provides an approximation for these potentials of mean force.

Ion-Solvent Interactions

Let us continue this theoretical development with a specific experimental system in mind – the immiscible liquid-liquid interface between an aqueous and an organic electrolyte solution – that we described previously. First, let's consider placing a single ion near the interface between pure water and pure organic liquid. As we described previously, in connection with Figure 18, the work to move this ion from a position z'' from the wall to a position z' is given by the difference in the potential of mean force at these positions $w_i(z') - w_i(z'')$.

Now recall that the potential of mean force is an excess chemical potential, that represents the change in intermolecular interactions when we add a particle to a system, where the term "excess" refers to an excess over the ideal part of the chemical potential that describes the change in configurational mixing entropy when adding the particle (refer to Eq. 33). If many ions are present in the system, then the potential of mean force just described represents only a part of the excess chemical potential, the part that I'll call the single ion potential of mean force, or $w_i^{sol}(z)$ (where the superscript refers to solvent, or single-ion/solvent interactions). During the past couple of decades, several authors have used molecular dynamics simulations to calculate $w_i^{sol}(z)$.

A variation of Eq. 34 can be written as

Eq. 80 $$f_i^{sol}(z') = -\frac{dw_i^{sol}(z')}{dz'},$$

where $f_i^{sol}(z')$ is the mean force on ion *i* at z' due to all of the solvent molecules. The single ion potential of mean force $w_i^{sol}(z)$ can be calculated in MD simulations by calculating the average force in the *z* direction for a range of values of *z*, then integrating,

Eq. 81 $$w_i^{sol}(z') = w_i^{sol,bulk} + \int_{z'}^{\infty} f_i^{sol}(z'')\, dz''$$

In practice, an ion is placed a distance *z* from an interface, as shown in Figure 38a, its position is constrained by a potential so that it stays within a small range Δz about *z*, then the force on it, $f_i^{sol}(z'')$, is computed.

(a) (b)

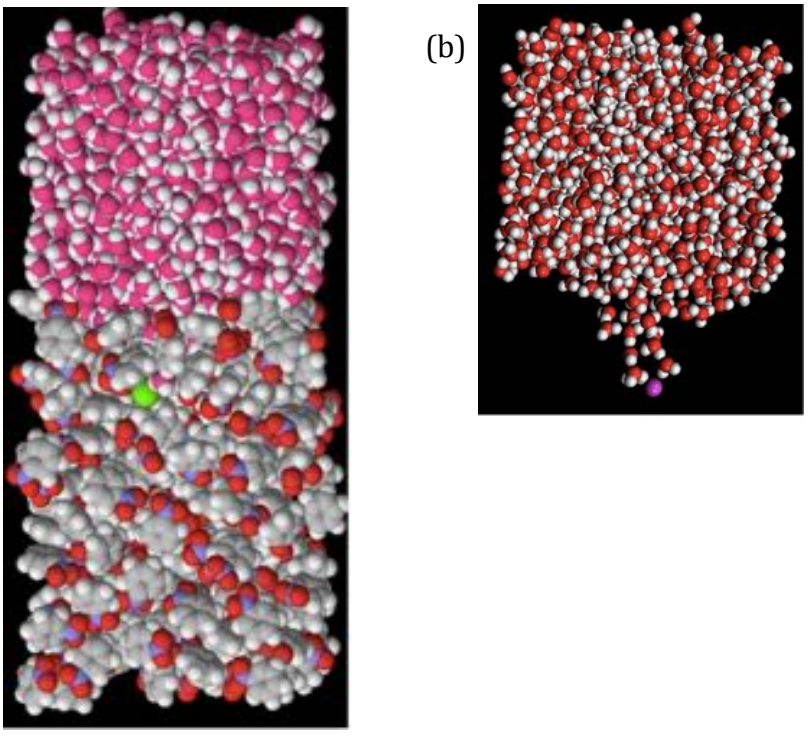

Figure 38 Cl^- ion at water/nitrobenzene liquid-liquid interface (from I. Chorny and I. Benjamin), see (Benjamin 1993) for related published work. Nitrobenzene phase is hidden in the image on the right.

Figure 38b illustrates one effect that can happen at a soft interface that influences $w_i^{sol}(z)$. Ions can drag their hydration through the interface with them. This leads to subtle effects in the simulated $w_i^{sol}(z)$ that have not been tested experimentally. Figure 39 illustrates the simulated values of $w_i^{sol}(z)$ for a related system that we have studied experimentally. Note that the Br^- and TBA^+ (tetrabutyl ammonium) potentials of mean

force are simulated, but the TPB^- (tetraphenyl borate) potential of mean force is an analytic form that is fit to x-ray data.

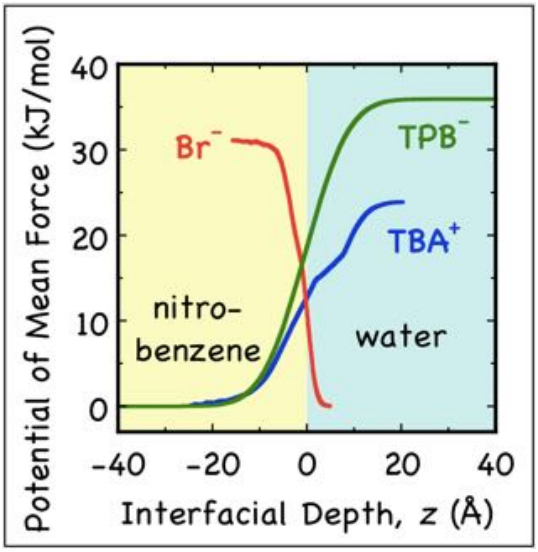

Figure 39 From (Luo et al. 2006b).

Within the context of density functional theory, we can write

Eq. 82 $$\frac{\beta}{A}\mathbf{\Omega}[c_+(z),c_-(z)] = \sum_{\pm}\left(\frac{\beta}{A}\mathbf{\Omega}^{PB}[c_i(z)] + \beta\int w_i^{sol}(z)c_i(z)\,dz\right)$$

Following the procedure of functional differentiation and minimization outlined in Eq. 77 through Eq. 79 yields (Luo et al. 2006b)

Eq. 83 $$c_\pm(z) = c_\pm^{bulk}\exp\left[\left(\mp e\phi(z) - w_i^{sol}(z)\right)/k_BT\right]$$

The ion distribution given by Eq. 83, along with the function $w_i^{sol}(z)$, can be substituted into Poisson's equation and numerically solved for $\phi(z)$ under appropriate boundary conditions. Subsequently, $c_\pm(z)$ can be calculated from Eq. 83 to yield ion distributions shown in Figure 40. Three features are immediately evident. First, the continuity of the ion concentrations through the interface in the potential of mean force (PMF) is the result of taking into account the structure of the soft interface. Second, the maximum concentrations for the potential of mean force (PMF) theory are much smaller than those for Poisson-Boltzmann theory. In fact, the contact concentrations $c(z=0)$ are unphysically large in Poisson-Boltzmann theory. As discussed before, this is primarily due to the effects of the

ion cavity that are neglected in Poisson-Boltzmann theory. Third, we see structure in $c_{TBA}(z)$ near the interface that appears to have a similar scale as the ion size (~ 1 nm).

Note that all of the ions are monovalent and the relative permittivity of nitrobenzene, 34.8, is about half that of water. This indicates that the Bjerrum length between ions in nitrobenzene is about twice that of ions in water. In comparison with our earlier discussion of monovalent and divalent ions in water, the Bjerrum length has an intermediate value (Bjerrum length of divalent ions in water will be 2^2=4 times larger than that of monovalent ions in water). This shows that the role of electrostatic interactions of monovalent ions in nitrobenzene will be more significant than for monovalent ions in water, but not as important as for divalent ions in water.

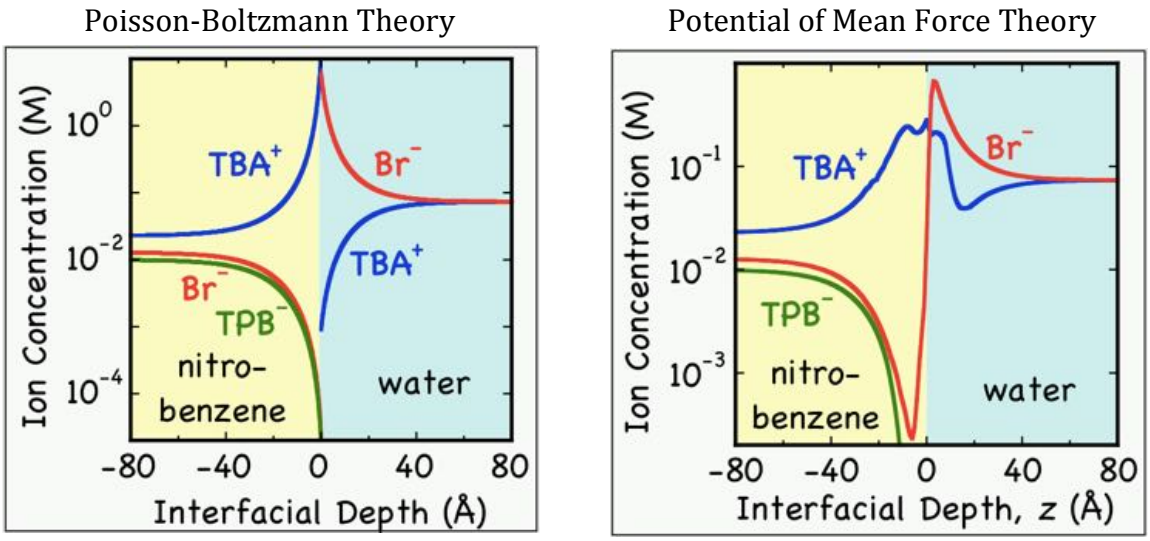

Figure 40 From (Luo et al. 2006b).

Predictions for ion concentrations can be tested by x-ray reflectivity experiments that probe the electron density profile. Since different ions have different electron densities that, themselves, differ from the electron density of the solvent, the ion concentrations shown in Figure 40 lead to an electron density profile $\rho_e(z)$. To a first approximation, the x-ray reflectivity can be expressed as the Fourier transform in reciprocal space of the gradient of the electron density $\rho_e(z)$ in the *z* direction (Pershan and Schlossman 2012),

Eq. 84
$$\frac{R(Q_z)}{R_F(Q_z)} \approx \left| \frac{1}{\Delta\rho_{e,bulk}} \int_{-\infty}^{+\infty} dz \frac{\partial \langle \rho_e(z) \rangle}{\partial z} \exp\left[-iQ_z z\right] \right|^2 ,$$

where the wave vector transfer $\vec{Q} = \vec{k}_s - \vec{k}_i = Q_z = \frac{4\pi}{\lambda}\sin\theta$ is in the *z*-direction for a reflectivity measurement. This means that reflectivity measures electron density variations in the *z*-direction. The scattering geometry is illustrated in Figure 41.

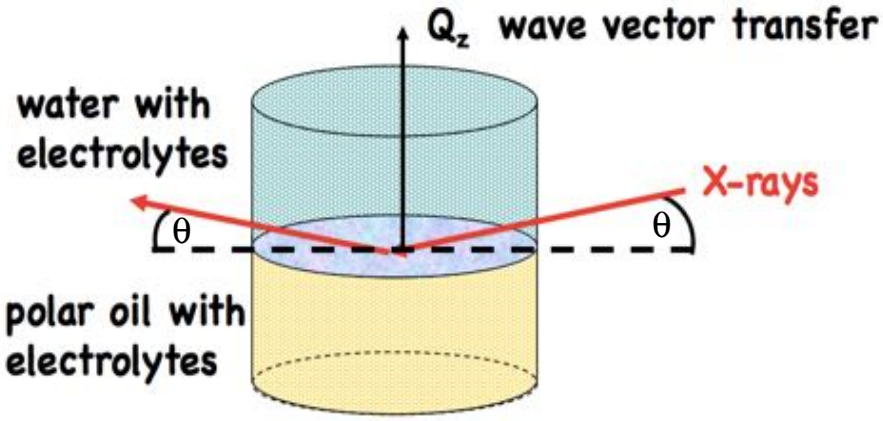

Figure 41

Measured reflectivity data and calculated reflectivity from the Poisson-Boltzmann (Gouy-Chapman) and PMF theory are illustrated in Figure 42 for five different initial concentrations of TBABr in water at a fixed initial concentration of TBATPB in nitrobenzene. This experiment takes advantage of the common ion technique described on p.43, for which $\Delta\phi^{w\text{-}o}$ is adjusted by choosing different initial electrolyte concentrations. The concentrations shown in Figure 42 produce a change in $\Delta\phi^{w\text{-}o}$ of about 30 mV. Although this is relatively small, we can see differences between the Poisson-Boltzmann and PMF theories. Note that there are not any adjustable parameters in the comparison made in Figure 42.

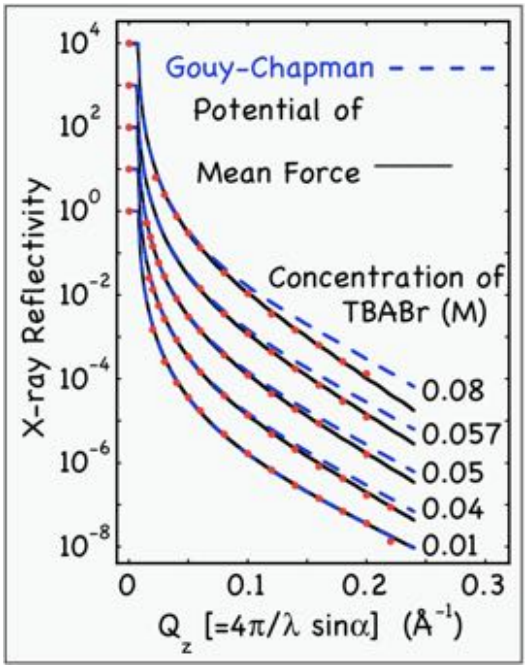

Figure 42 From (Luo et al. 2006b).

The Poisson-Boltzmann (Gouy-Chapman) theory works well at the lowest concentration (corresponding to $\Delta\phi^{w\text{-}o} =$ -0.245 V) with successively larger variations as the concentration is raised to the largest concentration that has $\Delta\phi^{w\text{-}o} =$ -0.277 V. Although the differences still appear small because of the logarithmic scale, the difference between theory and experiment at the largest concentration are equivalent to 25 experimental standard deviations through the full range of Q_z. Further details of this experiment can be found in two papers (Luo et al. 2006b, a).

Ion-Ion Correlations

The experiment just discussed did not reveal a strong dependence on ion correlations mediated by strong electrostatic interactions, as shown in (Luo et al. 2006a). This is consistent with the coupling strength $\Gamma < 1$ for this experiment (recall Eq. 26). Another experiment that we did a few years ago used a polarizable interface (see pp. 43-44) in an electrochemical cell. This system, illustrated in Figure 36, allowed $\Delta\phi^{w\text{-}o}$ to be varied over a range of ±400 mV that is much larger than the 30 mV change achievable with the unpolarizable interface discussed previously.

Importantly, this newer experiment used 1,2-dichloroethane (abbreviated as DCE) as the organic phase, which has a relative permittivity of 10.4. Therefore monovalent ions in DCE have a Bjerrum length similar to that of trivalent ions in water. This allowed us to tune the coupling strength to be as large as $\Gamma = \ell_B / d \approx 4$, so large electrostatic effects are expected.

Another way to view this experiment is that tuning $\Delta\phi^{w\text{-}o}$ changes the ion density near the interface, see Figure 36, which changes the average distance *d* between ions near the interface, thus tuning the coupling strength $\Gamma = \ell_B / d$. Essentially, this experiment allows us to tune ion correlations. When the coupling strengths are greater than 1, we expect strong electrostatic interactions and the Poisson-Boltzmann theory should fail. This is evident in Figure 43.

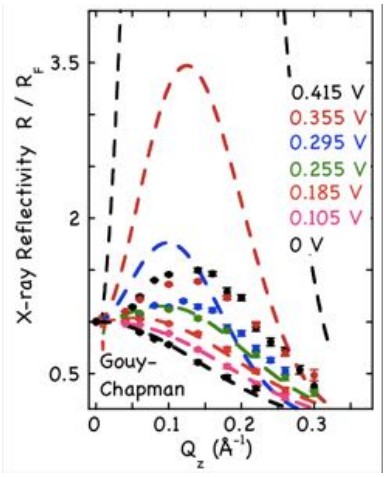

Figure 43 Poisson-Boltzmann (Gouy-Chapman) theory and data from experimental system shown in Figure 36, unpublished figure.

The PMF theory also fails to match the data, though not as dramatically, see Figure 44.

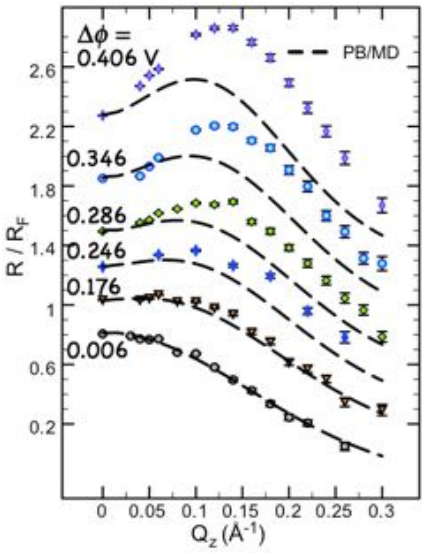

Figure 44 PMF theory and data from experimental system shown in Figure 36, (Laanait et al. 2012).

Since the coupling strength in this system is large, we need to include ion-ion correlation effects explicitly in our theory. We can do this by generalizing Eq. 82 to include the effect of correlations between ions, which were discussed earlier in the section on many body effects

Eq. 85 $$\frac{\beta}{A}\mathbf{\Omega}[c_+(z),c_-(z)]=\sum_{\pm}\left(\frac{\beta}{A}\mathbf{\Omega}^{PB}[c_i(z)]+\beta\int w_i^{sol}(z)c_i(z)\,dz+\beta\int w_i^{ion-ion}(z)c_i(z)\,dz\right),$$

if we can identify the piece of the potential of mean force $w_i^{ion-ion}(z)$ that describes ion-ion correlations. Alternatively, we could have written the last term as $(\beta/A)F_i^{ion-ion}[c_i(z)]$, where $F_i^{ion-ion}[c_i(z)]$ represents a correlation free energy, that is related to $w_i^{ion-ion}(z)$ by

Eq. 86 $$\frac{\delta F_i^{ion-ion}[c_i(z)]}{\delta c_i(z)}.$$

Similar to the differentiation and minimization of Eq. 82, a similar procedure will lead to an expression for the ion distributions given by

Eq. 87 $$c_\pm(z)=c_\pm^{bulk}\exp\left[\left(\mp e\phi(z)-w_i^{sol}(z)-w_i^{ion-ion}(z)\right)/k_BT\right]$$

Although there has been a substantial theoretical effort to develop theories that describe correlations, all of them are beyond the scope of these lectures. Nevertheless, we

have used two different approaches to evaluate $F_i^{ion-ion}[c_i(z)]$, one by Roland Kjellander referred to as the anisotropic hypernetted chain (AHNC) method (Kjellander and Marcelja 1985), and the other developed by a series of authors, but assembled in the form that we used by Yan Levin and co-authors (Diehl et al. 1999), (see (Luo et al. 2006a) and (Laanait et al. 2012) for implementation of these methods in the context of analyzing the experiments discussed here). The latter method is based upon the Debye-Hückel hole model within the context of the one component plasma and uses a weighted density approximation. Since we use a one component plasma, we can describe ion-ion correlations for only one of the ionic species. This limitation does not apply to the AHNC method, though it is more complicated to apply. Unfortunately, both methods are too complicated to adequately review in this course. Nevertheless, I introduced Eq. 85, in spite of these complications, because it provides a way to account for both solvent and ion-ion correlation effects, as shown in Figure 45.

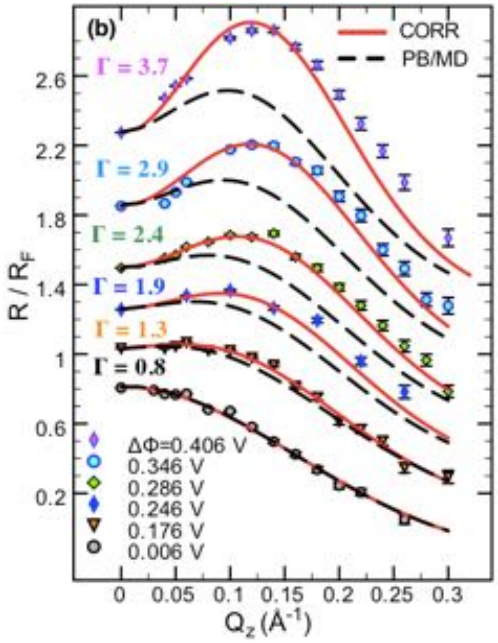

Figure 45 Red line includes the effect of ion-ion correlations, dashed line neglects them. Data is measured from the experimental system shown in Figure 36, (Laanait et al. 2012). There are not any adjustable parameters in the theory.

Now, what about the electrochemists, who like to measure capacity, or similarly, the excess surface charge at the interface? Figure 46 shows that this approach works well to describe the measured excess charge for this system (measured from the interfacial tension, as described in Eq. 67). Again, there are not any adjustable parameters in the theory.

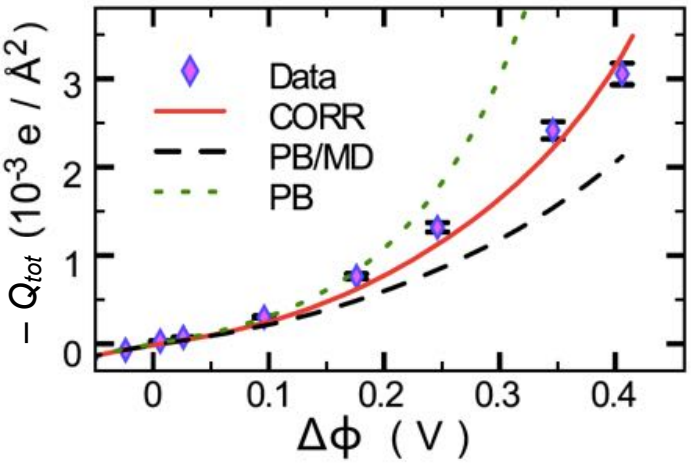

Figure 46 Short-dashed green line is Poisson-Boltzmann theory; long-dashed black line includes the single ion potential of mean force, which accounts for the structure of the soft liquid-liquid interface; red line also includes the ion-ion correlations or many body effects (Laanait et al. 2012).

Summary

Thanks for listening to this extended story that started with Poisson-Boltzmann theory, explored the role of many body effects on ion distributions, then proceeded to a hybrid approach within the framework of density functional theory that allowed us to describe ion distributions at a model soft interface, the electrified liquid-liquid interface. I regret the many things that I've had to leave out, especially some reasonable successes of Poisson-Boltzmann theory and a broader view of current research activity within this field. Nevertheless, I hope that I have stimulated your interest.

References and Recommendations for Further Reading

Andelman D (2006) Introduction to electrostatics in soft and biological matter. In: Andelman D, Poon WCK (eds) Soft Condensed Matter Physics in Molecular and Cell Biology. Taylor & Francis, New York.

Benjamin I (1993) Mechanism and dynamics of ion transfer across a liquid-liquid interface. Science 261:1558.

Bera MK, Chan H, Moyano DF, Yu H, Tatur S, Amoanu D, Bu W, Rotello VM, Meron M, Kral P, Lin B, Schlossman ML (2014) Interfacial transport and voltage-tunable arrays of charged nanoparticles. Nano Lett 14:6816-6822.

Besteman K, Eijk Kv, Vilfan ID, Ziese U, Lemay SG (2007) Influence of Charged Surfaces on the Morphology of DNA Condensed with Multivalent Ions. Biopolymers 87:141-148.

Besteman K, Zevenbergen MAG, Heering HA, Lemay SG (2004) Direct observation of charge inversion by multivalent ions as a universal electrostatic phenomenon. Phys Rev Lett 93 (17):170802.

Carlton RJ, Ma CD, Gupta JK, Abbott NL (2012) Influence of Specific Anions on the Orientational Ordering of Thermotropic Liquid Crystals at Aqueous Interfaces. Langmuir 28:12796-12805.

Diehl A, Tamashiro MN, Barbosa MC, Levin Y (1999) Density-functional theory for attraction between like-charged plates. Physica A 274:433-445.

French RH, Parsegion VA, Podgornik R, Rajter RF, Jagota A, Luo J, Asthagiri D, Chaudhury MK, Chiang Y-M, Granick S, Kalinin S, Kardar M, Kjellander R, Langreth DC, Lewis J, Lustig S, Wesolowski D, Wettlaufer JS, Ching W-Y, Finnis M, Houlihan F, Lilienfeld OAv, Oss CJv, Zemb T (2010) Long range interactions in nanoscale science. Rev Mod Phys 82:1887-1944.

Girault HH (2004) Analytical and Physical Electrochemistry. EPFL Press, Lausanne, Switzerland.

Girault HHJ, Schiffrin DJ (1986) A New Approach for the Definition of Galvani Potential Scales and Ionic Gibbs Energies of Transfer across Liquid-Liquid Interfaces. Electochimica Acta 31 (10):1341-1342.

Hou B, Laanait N, Yu H, Bu W, Chen C-H, Yoon J, Lin B, Luo G, Vanysek P, Schlossman ML (2013) Ion distributions at the water/1,2-dichloroethane interface: Potential of mean force approach to analyzing X-ray reflectivity and interfacial tension measurements J Phys Chem B 117:5365-5378.

Kjellander R, Greberg H (1998) Mechanisms behind concentration profiles illustrated by charge and concentration distributions around ions in double layers. J Electroanal Chem 450:233-251.

Kjellander R, Marcelja S (1985) Inhomogeneous Coulomb Fluids with Image Interactions Between Planar Surfaces. I. J Chem Phys 82 (4):2122-2135.

Koltover I, Wagner K, Safinya CR (2000) DNA condensation in two dimensions. Proc Nat Acad Sci (USA) 97:14046–14051.

Laanait N (2013) Ion Correlations at Electrified Soft Matter Interfaces. Springer Theses. Springer, London.

Laanait N, Mihaylov M, Hou B, Yu H, Vanysek P, Meron M, Lin B, Benjamin I, Schlossman ML (2012) Tuning Ion Correlations at an Electrified Soft Interface. Proc Nat Acad Sci (USA) 109:20326-20331.

Levin Y, Santos APd, Diehl A (2009) Ions at the Air-Water Interface: An End to a Hundred-Year-Old Mystery? Phys Rev Lett 103:257802-1 - 257802-4.
Luo G, Malkova S, Yoon J, Schultz DG, Lin B, Meron M, Benjamin I, Vanysek P, Schlossman ML (2006a) Ion Distributions at the Nitrobenzene-Water Interface Electrified by a Common Ion. J Electroanal Chem 593:142-158.
Luo G, Malkova S, Yoon J, Schultz DG, Lin B, Meron M, Benjamin I, Vanysek P, Schlossman ML (2006b) Ion Distributions Near a Liquid-Liquid Interface. Science 311:216-218.
Messina R, Holm C, Kremer K (2001) Strong electrostatic interactions in spherical colloidal systems. Phys Rev E 64:021405.
Pershan PS, Schlossman ML (2012) Liquid Surfaces and Interfaces: Synchrotron X-ray Methods. Cambridge University Press, Cambridge.
Rouzina I, Bloomfield VA (1996) Macroion Attraction due to Electrostatic Correlation between Screening Counterions. 1. Mobile Surface-Adsorbed Ions and Diffuse Ion Cloud. J Phys Chem 100:9977–9989.
Zhang YJ, Cremer PS (2010) Chemistry of Hofmeister Anions and Osmolytes. Annu Rev Phys Chem 61:63-83.